FIRST PRINCIPLES STUDY OF PROPERTIES OF THE OXIDIZED CU(100) AND CU(110)

by

ANTOINE OLENGA

Presented to the Faculty of the Graduate School of
The University of Texas at Arlington in Partial Fulfillment
of the Requirements
for the Degree of

MASTER OF SCIENCE IN PHYSICS

THE UNIVERSITY OF TEXAS AT ARLINGTON

May 2013

Acknowledgements

I want to thank everyone who contributed to the realization of this work and to my formation. Especially, I want to express my gratitude to Dr. Fazleev who was the supervisor of this work. I appreciate his encouragement and patience during our meetings and discussions. I want also to thank all personal of the Physics Department of UTA for their assistance.

April 04, 2013

Abstract

FIRST PRINCIPLES STUDY OF PROPERTIES OF

THE OXIDIZED CU(100) AND

CU(110)

Antoine Olenga, M.S.

The University of Texas at Arlington, 2013

Supervising Professor: NAIL FAZLEEV

Copper based catalysts are of importance to a number of industrial processes including the synthesis of methanol, the reduction and decomposition of nitrogen oxides, and treatment of waste water. In copper catalysis surface oxidation and oxidic overlayers are believed to play a crucial role. In this work using density functional theory (DFT) within the generalized gradient approximation (GGA) we have studied the stability and associated electronic properties of the oxidized Cu(100) and Cu(110) surfaces. Especially, we have focused on studies of changes in the interlayer spacing, electron work function, binding energy, and density of states with oxygen coverage. We have examined the cases of various oxygen coverages of the non-reconstructed, missing row reconstructed Cu(100), and added row reconstructed Cu (110) surfaces. The first-

principles calculations in this work have been performed using DMOl3 code. The obtained theoretical results have

Table of Contents

List of Illustrations

List of Tables

Chapter 1

Introduction

The physical properties of copper have been used by humans in many aspects of the life since the ancient times. Today, copper has been used in the manufacturing of electrical compounds in microelectronics, and in the many other applications. The oxidation of copper is inevitable due to our industrial needs, so the understanding of the mechanism of oxidation is of a great importance. It is through its surface that a crystal reacts with foreign atoms, so to understand the mechanism of oxidation one should start by understanding how the copper surface interacts with the oxygen atoms. Due to its interaction with oxygen atoms, the arrangement of copper surface atoms is altered, and the surface undergoes relaxation and reconstruction. While the relaxation involves small modification of the arrangements of the atoms on and near the surface, the reconstruction involves larger displacement of the atoms and the change in the periodicity of the surface. Both the relaxation and reconstruction may occur with clean surfaces in high vacuum. They may also be induced by the adsorption of the other atoms onto the surface. Both relaxation and reconstruction may cause the modification of the electronic properties of the surface. During the reconstruction the oxygen atoms may stay on the surface or penetrate bellow the first atomic layers of the copper. In this present work we were interested in the reconstruction of the Cu(100) and

Cu(110) surfaces due to adsorption of oxygen atoms. It is known that these two surfaces reconstruct differently. With the increase of the oxygen coverage, the Cu (100) surface undergo a special reconstruction called “Missing Row” reconstruction, and the Cu(110) undergo the “Added row reconstruction. The coverage at which each of these surfaces transform to reconstructed surface, how far the oxygen atoms can penetrate into the copper atomic layers, the displacement of the copper atoms compared to their bulk positions, and the change in the electronic properties have been subjects of debate. Even though some answers have been provided, we still need to conduct more studies to understand fully the oxidation process. In this work, we performed some calculations to understand how the reconstructions of the Cu(100) and Cu(110) surface take place, and how those reconstruction modify the electronic properties of the Cu(100) and Cu(110) surfaces. Among the properties that we have examined include the atomic interlayer spacing, the density of states, the work function, and charge density. Our work is divided into three parts. In the first chapter we describe the DFT as implemented in DMol3 software, which is the software we used for our calculations, in the second part we explain our calculations and the results we obtained, and the last part is a short conclusion. In the second part, we present our results on clean surfaces. The work is divided into six chapters: Introduction, Theory, Clean Surfaces, Oxygen Adsorption on the Cu(100) surface, Oxygen adsorption on the Cu(110) surface, and Conclusion.

In second chapter we gave a short description of the DFT as implemented in the DMol3 code, in the chapter 3 we gave short details of the three miller index surfaces and the computational details, in the chapter 4 we treated the case of oxygen adsorption on Cu(100) surface, and in the chapter 5 we talked about the adsorption of the oxygen on the Cu(110) surface. As method we used the Density Functional Theory (DFT) within the Generalized Gradient Approximation (GGA). All calculations were used using the DMol3 Code, and the Material Studio software was used in the building the structures and analyzing the results.

Chapter 2

Theoretical Approach

2.1 Introduction

The DFT is the most useful and available method for solving a system of interacting electrons. This theory finds its foundation in the Hohenber theorem. Its characteristic is that it tries to find the electron density distribution instead of trying to solve the Schrodinger equation and find a wave function for many-body system. In a few words, the DFT allows us to calculate the ground state properties, including the total energy, starting from the charge distribution. In this part, a short summary of the DFT as implemented in the DMol3 is explained.

2.2 Solution of Many-Body Problem

In Quantum Mechanics, the wave function gives all information we can get about a system. The wave function is obtained by solving the Schrodinger equation. In condensed matter we deal with systems with large numbers of particles and solving the Schrodinger equation for these systems is not an easy task, so we need to relate the description of those systems to the solution of the problem for a single of one particle which is easier to solve.

For a system with a single electron moving in a region where the potential is $v(r)$, the wave function $\varphi(r)$ is found by solving the following single particle Schrodinger's equation.

$$\left[-\frac{\hbar^2\nabla^2}{2m}+v(\vec{r})\right]\varphi(\vec{r}) = \varepsilon\varphi(\vec{r}) \quad (1)$$

This equation is simple to solve. When the number of electrons becomes more than one, we are to deal with a many-body problem.

The time independent Schrodinger equation for the many-body system can be written as follows:

$$\hat{T}\psi_{MB}+\hat{V}\psi_{MB}=E\psi_{MB} \quad (2)$$

In this expression ψ_{MB} is the many-body wave function, $\hat{\mathrm{T}}$ is the many-body kinetic energy, and $\hat{V}$ the many-body potential energy.

ψ_{MB}=$\psi_{MB}(r_1, r_2, \dots, r_n, R_1, R_2, \dots, R_N)$ where r_i and R_j coordinates of electrons and nuclei coordinates. The many-body kinetic energy is given by the following equation.

$$\hat{T} = -\frac{1}{2}\hbar^2\left\{\sum_i\frac{\nabla_{r_i}^2}{m_i}+\sum_j\frac{\nabla_{R_j}^2}{M_j}\right\} \quad (3)$$

where the m_i and M_j are the masses of electrons and the nuclei respectively. The many-body potential energy operator is given by:

$$\hat{V} = \frac{1}{2}\sum_{i\neq j}\frac{e^2}{|r_i-r_j|}-\sum_{i,j}\frac{Z_j e^2}{|r_i-R_j|}+\frac{1}{2}\sum_{i\neq j}\frac{Z_i Z_j e^2}{|R_i-R_j|} \quad (4)$$

where $Z_j e$ is the electric charge of the nucleus j.

Since the masses of the nuclei are much greater than those of the electrons we can consider the nuclei to be in rest and use the Born-Oppenheimer approximation. In this case the electrons are considered moving in an external

potential created by the positively charged nuclei. Therefore the Schrodinger equation (2) reduces to the following equation where we also dropped the potential energy due to the nucleus-nucleus interactions.

$$\left\{-\frac{1}{2}\hbar^2\sum_i\frac{\nabla_{\vec{r}_i}^2}{m_i}+\frac{1}{2}\sum_{i\neq j}\frac{e^2}{|r_i-r_j|}-\sum_{i,j}\frac{Z_je^2}{|r_i-R_j|}\right\}\psi_{MB}=E\psi_{MB} \quad (5)$$

The solution of equation (5) depends parametrically on the nuclei coordinates. Since now the solution depends only on the electrons coordinates and the electrons are all identical, the wave function describing the electrons state becomes

$$\psi_{MB}=\psi(\vec{r}_1,\vec{r}_2,\dots,\vec{r}_n).$$

Now the Schrodinger equation for the system of n electrons moving in the potential created by the nuclei can be written as:

$$\left[\sum_{\mathrm{i}}^{\mathrm{n}}\left(-\frac{\hbar^2\nabla^2}{2\mathrm{m}}-\frac{\mathrm{Z_k e^2}}{|\vec{\mathrm{r}}_{\mathrm{i}}-\vec{\mathrm{R}}_{\mathrm{k}}|}\right)+\frac{1}{2}\sum_{\mathrm{i}\neq j}\frac{\mathrm{e}^2}{|\vec{\mathrm{r}}_{\mathrm{i}}-\vec{\mathrm{r}}_{\mathrm{j}}|}\right]\psi_{MB}=\mathrm{E}\psi_{MB} \quad (6)$$

In this equation, n is the number of electrons, k extends over all nuclei in the system.

$U(r_i,r_j)=\sum_{i\neq j}\frac{e^2}{|\vec{r}_i-\vec{r}_j|}$ is the electron-electron interactions,

$T=-\frac{\hbar^2}{2m}\sum_i\nabla^2{}_i$ is the sum of the electrons kinetic energies, and

V= $\sum_i v(\vec{r}_i)=\sum_{ik}\frac{Z_ke^2}{|\vec{r}_i-\vec{R}_k|}$ is the sum of the potential energy due to nucleus-electron interactions.

Solving this equation is not an easy task since we need to sum the contributions from all electrons, and we know that in condensed matter we deal with systems with large numbers of electrons and nuclei. The kinetic energy term T which represents the kinetic energy of interacting electrons also poses problem because it cannot be expressed explicitly. Therefore some approximations have proposed to solve the problem among which are the Thomas Fermi approximation, the Local Density Approximation (LDA), Local Spin Density Approximation (LSDA), Non Local Density approximation , and the GGA approximation. All those approximations try to we express the many body wave function ψ_{MB} in terms of one particle wave function equation $\varphi(\vec{r})$ defined in the equation (1).

The Thomas-Fermi approximation:

The Thomas-Fermi approximation was the first attempt to use the density to obtain information about electronic and atomic system. In this approximation for non interacting system the kinetic energy is function of the local electron density, and it expressed as:

$$T_{TF}[\rho] = C_F \int \rho^{5/3}(\vec{r}) d^3(\vec{r}) \quad (7)$$

And the total energy is

$$E_{TF}\left[\rho\overrightarrow{(r)}\right] = C_F \int \rho^{5/3}(\vec{r}) d^3(\vec{r}) - Z \int \frac{\rho\overrightarrow{(r)}}{\overrightarrow{(r)}} d^3\,\vec{r} + \frac{1}{2} \int \frac{\rho(\vec{r}_1)(\vec{r}_2)}{|\vec{r}_1 - \vec{r}_2|} d^3\vec{r}_1 d^3\vec{r}_2$$

2.3 Exchange-Correlation Energy

In order to express the many-body wave equation in terms of one particle wave function we use the approximations that allow us to write the total energy of the system as follows:

$$E_T[\rho] = T[\rho] + \mathrm{U}[\rho] + E_{xc}[\rho] \quad (8)$$

where $T[\rho]$ is the kinetic energy of a system of non interacting particles of density ρ, $\mathrm{U}[\rho]$ is the electrostatic energy due to Coulombic interactions, and the $E_{xc}[\rho]$ is the term that includes all many-body contributions to the total energy. E_{xc} is called exchange-correlation energy. Approximations are used to express estimate the $E_{xc}[\rho]$ term.

2.2.1 Local Density Approximation(LDA)

The most important type of approximations is the local-density approximation (LDA). In the LDA approximation, they use the assumption that the charge density varies slowly around any given point. Therefore for any point inside a volume element centered at a point A, the exchange correlation energy depends on charge density at point A only. With this assumption that E_{XC} is obtained by integrating the electron gas.

$$E_{XC} \cong \int \rho(\vec{r})\, \varepsilon_{xc}^{0}\left[\left(\rho(\vec{r})\right)\right] d\vec{r} \quad (9)$$

Where ε_{xc}^{0} [ρ] is the exchange-correlation energy per particle in a uniform electron gas and ρ is the number of particles. The LDA is based on the known exchange-correlation energy of the uniform electron gas. The LDA approximation

is good for slowing varying systems and high density systems, but it is bad for very few electron systems.

2.2.2 Local Spin-Density Approximation (LSDA)

In the equation (9) we did not take account of the fact that we may have unpaired electrons. To take into account the different contribution to exchange -correlation energy of electrons of the same energy but with different spins, we use the Local Spin Density Approximation. By doing so we need to consider two densities: $\rho_{\downarrow}(\vec{r})$ and $\rho_{\uparrow}(\vec{r})$ in the calculations of the E_{XC}. In this approximation the Exchange correlation energy is written as follow:

$$E_{XC}^{LSDA}\left(\rho_{\downarrow}(\vec{r}),\rho_{\uparrow}(\vec{r})\right) = \int \rho(\vec{r})\, \varepsilon_{xc}^{0}[\rho_{\downarrow}(\vec{r}),\rho_{\uparrow}(\vec{r})\,]\, d\vec{r} \quad (10)$$

where $\varepsilon_{xc}^{0}$is the exchange-correlation energy/particle of the homogeny electrons gas.

2.2.3 Generalized Gradient Approximation (GGA)

In the LDA we assume that the density at any point is known. In any real system the density is a spatially varying function. The Generalized Gradient Approximation (GGA) takes into account the non homogeneity of the electron gas. In this approximation one tries to calculate the gradient-corrections to the LDA approximation. In order to improve the LDA in some cases, we need to introduce into the $\varepsilon_{xc}[\rho]$ expression terms that take into account the non homogeneity of the charge density. Thus the Exc is expressed as functional of the charge density and the gradient of the charge density.

$\varepsilon_{xc}^{GGA}=\int d^3rf(n(\boldsymbol{r}),\nabla n(r))$ (11)

$E_{GGA} = E_{LSD} + E_x^G + E_c^G$ (12)

In DMol3 calculations different GGA approximations are proposed, and each differs from another by the choice of the function $f(n(\boldsymbol{r}),\nabla n(r))$.

The equation can be written as:

For Becke GGA

$E_x^G = b\sum_\sigma \int \frac{\rho_\sigma x_\sigma^2\, dr}{1+6bx_\sigma \sinh^{-1} x_\sigma}$ (13)

For Pedew GGA

$E_c^G = \int f(\rho_\downarrow,\rho_\uparrow)\, e^{-g(\rho)|\nabla_\rho|}\left|\nabla_\rho\right|^2 dr$ (14)

With one of these approximations the total energy can be written as follows:

E(ρ) = $\sum_i \left[\phi_i \left|\frac{-\hbar^2\nabla^2}{2m}\right| \phi_i\right]$ + $\langle\, \rho(r_1\,)[\varepsilon_{xc}\,[\rho(r_1)] + \frac{V_e(r_1)}{2} - V_N]\,\rangle$, that can be also written:

$E[\rho(\vec{r})] = T_0[\rho(\vec{r})]+\int V_{ext}\,\rho(\vec{r})\,d\vec{r} + \int \frac{\rho(\vec{r})\rho(\overrightarrow{r'})}{\left[\vec{r}-\overrightarrow{r'}\right]}\, d\vec{r}d\overrightarrow{r'} + E_{xc}\left[\rho(\overrightarrow{r})\right]$

(15)

2.3 Honenberg Kohn Theorem[..]

The Hohenberg-Kohn theorem states that all ground state properties, and particularly the total energy are functional of the charge density.

$E[\psi(\vec{r}_1,\dots,\vec{r}_N)] = E[\rho(\vec{r})]$

$$\mathrm{E}[\rho] = T_0[\rho] + U[\rho] + E_{xc}[\rho]$$

According to the Hohenberg-Kohn theorem, all electronic properties of a system of N interacting electrons in an external potential V(r) are completely determined by the electronic charge density. In other words, the external potential is a unique functional of the electron density. That also means that the Hamiltonian, and hence all ground state properties, are determined solely by the electron density.

The Hohenberg-Kohn Theorem provides a method of determining the total energy and some other properties of the system by replacing the multi-function electronic wave function with the electron density which is a function of just three variables only; therefore easier to handle.

2.4 Khon-Sham Equations

Kohn and Sham proposed a way to solve a many body problem. Their equations are used to substitute a system of interacting particles with a system of non-interacting particles that has the same density as the interacting system. To understand that $\mathrm{E}(\rho)$ needs to be optimized with respect to ρ in the equation (15). Applying the variation principle to this equation, we get

$$\frac{\delta E[\rho(\vec{r})]}{\delta\rho(\vec{r})} = \frac{\delta T_0[\rho(\vec{r})]}{\delta\rho(\vec{r})} + V_{ext}(\vec{r}) + \int \frac{\rho(\overrightarrow{r'})}{[\vec{r}-\overrightarrow{r'}]} d\overrightarrow{r'} + \frac{\delta E_{xc}[\rho(\overrightarrow{r})]}{\delta(\overrightarrow{r})} = \quad 0. \qquad (16)$$

$V_{xc}[\rho(\vec{r})] = \frac{\delta E_{xc}[\rho(\vec{r})]}{\delta(\vec{r})}$ is the exchange correlation potential, $V_H[\rho(\vec{r})] = \frac{1}{2}$

$\int \frac{\rho(\vec{r'})}{[\vec{r}-\vec{r'}]} d\vec{r'}$ is the Hartree potential, and $V_{eff}(\vec{r}) = V_{ext}(\vec{r}) + V_H[\rho(\vec{r})] +$

$V_{xc}[\rho(\vec{r})]$

That leads to coupled equations proposed by Kohn and Sham.

$$\left[\frac{-\hbar^2\nabla^2}{2m} + V_{eff}[\rho(\vec{r})]\right]\varphi_i(\vec{r}) = \varepsilon_i^{HK}\varphi_i(\vec{r}) \qquad (17)$$

The $\varphi_i(\vec{r})$ and ε_i^{HK} are the orbital and energy eigenvalues.

These equations need to be solved by self consistently to find the density that minimizes the total energy, knowing that $\rho(\vec{r}) = \sum_i \langle\varphi_i|\varphi_i\rangle$.

2.5 DMol3 Method and Algorithm

DMol3 uses self-consistent method to calculate the density and the energy that corresponds to a specific atomic arrangement in the solid. The Energy calculations are done by following the following steps.

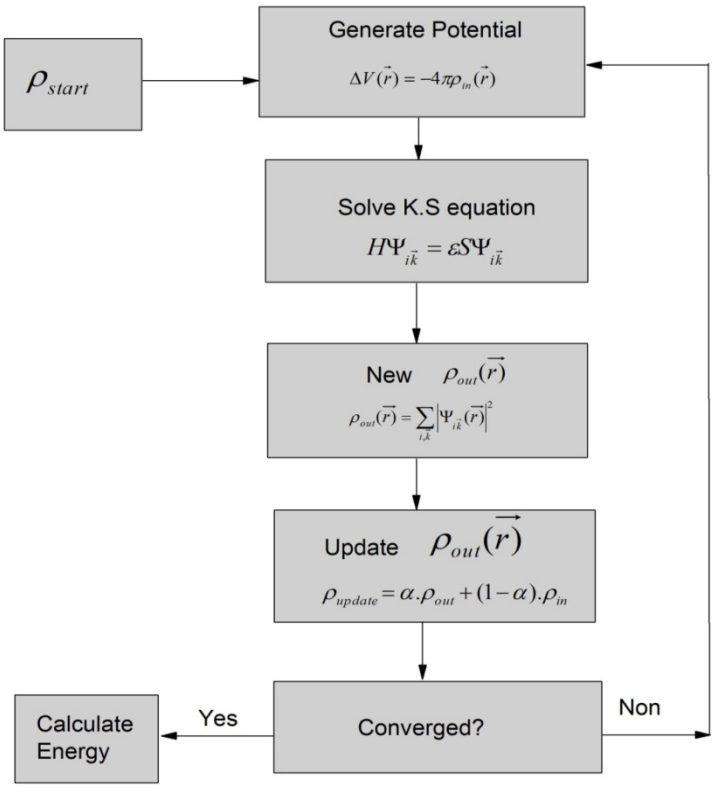

Figure 2-1 Self consistent flowchart

If the geometry optimization is required, more steps need to be added to the previous algorithm. The geometry optimization is defined as an iterative process in which the positions of atoms are readjusted until they reach a stable geometry, which corresponds to the minimum energy. DMol3 use algorithms that are not under control of the user to readjust the positions of atoms. Each step of the geometry optimization requires also the calculation of different energies, including total energy, binding energy, Fermi energy, etc. The output files contain the results of calculations for each step of the optimization step. The user fixes the

tolerance atoms displacement, energy, and maximum gradient. The job will stop when those combined tolerances are reached. The steps followed by geometry optimization are given in the following figure.

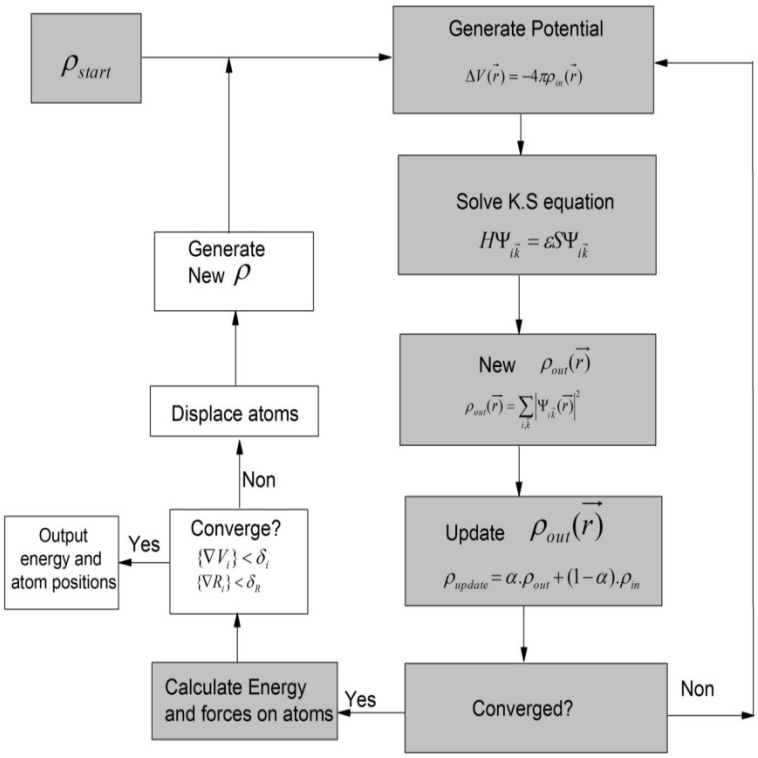

Figure 2-2 Geometry optimization flowchart

The Fig 2-2 shows a chart of geometry optimization we realized on all the structures in this work. The tolerances on the energy change, maximum force and maximum displacement were respectively 0.0000200 Ha, 0.004 Ha/Angstrom, and 0.005 Angstrom. Fig 2.3 shows the energy evolution, the maximum displacement, and the maximum force during the geometry optimization of the

Cu(110) clean surface. We can see that all the three convergence criteria were satisfied after 20 optimizations steps.

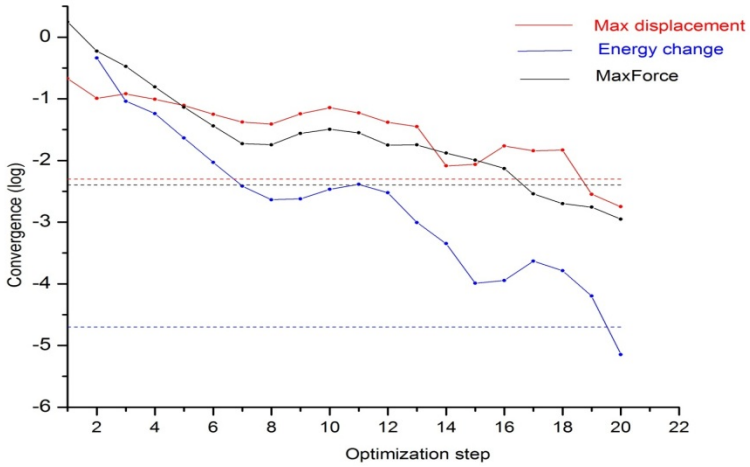

Figure 2-3 Example of geometry optimization

2.6 Some Important Parameters

In order to get an accurate result from DMol3 calculations, some parameters need to be assigned values. Here we explain some of the important parameters and what the values we assigned to them in our calculation.

2.6.1 K-Points and Brillouin Zone Sampling

The energy calculation is done in the reciprocal space. The Fourier Transform (FT) is used to change from real space to reciprocal space, and after calculations are done the inverse FT is used to return back to real space. Therefore the BZ sampling is important in our calculations. The k-points set is used to define the accuracy of the Brillouin Zone (BZ) sampling.

The Bloch Theorem is given by the following equation

$$\varphi_{n\vec{k}}(\vec{r}) = \exp\left(i.\vec{k}\vec{r}\right) u_{n\vec{k}}(\vec{r}) \qquad (18)$$

where $\vec{r} = n_1\overrightarrow{a_1} + n_2\overrightarrow{a_2} + n_3\overrightarrow{a_3}$ and $\vec{k} = k_1\overrightarrow{g_1} + k_2\overrightarrow{g_2} + k_3\overrightarrow{g_3}$.

The $\{\overrightarrow{a_i}\}$ and$\{\overrightarrow{g_i}\}$ are respectively the real space and reciprocal lattice vectors, and n_i are integers. The equation (18) can be satisfied by an infinite number of $\vec{k}$ = $\vec{k}'$+ $\vec{G}$, so we can limit ourselves to the values of $\vec{k}$ which lie within the first BZ. Then in order to construct the density we need to calculate the Hamiltonian eigenstate from each allowed value of k within the BZ. In practice only a finite number of points need to be chosen [04]. The k-points set is a set of three numbers used to define the accuracy of the B.Z. The user can control the number of divisions along each axis of the reciprocal lattice vectors by choosing k_1 k_2 and k_3 so that the total number of k-points is $k_1.k_2.k_3$. Monkhorst and Pack [04] developed a method for reducing the number of k-points and producing a uniform grid of points along the three axes in reciprocal space.

The choice of k-points depends on the length of each lattice vector. Since we have $\overrightarrow{a_i}.\overrightarrow{g_j}.$ =2 $\pi\delta_{ij}$, the volume of the supercell V is related to the volume of the Brillouin zone Ω by

$$\Omega = \frac{(2\pi)^3}{V}$$

$$\overrightarrow{a_i} = 2\pi\frac{\overrightarrow{g_j}\Lambda\overrightarrow{g_k}}{V} \quad \text{where } V = \overrightarrow{a_1}.(\overrightarrow{a_2}\,\Lambda\overrightarrow{a_3})$$

The BZ is very small for large system because the two volumes are inversely proportional. Therefore the k-points need to be chosen by taking

account of the length of the $\vec{a_i}$. The larger is$|\vec{a_i}|$, the smaller should be the k-points number in that directions. In this work the choice of k points set was based on the dimensions of the supercell and the precision we want to achieve.

2.6.2 Basis

DMol3 uses a Linear Combination of Atomic Orbitals (LCAO) method.

$$\Psi_i = \sum_\alpha \sum_j C_{ij}^\alpha \phi_j^\alpha(r_\alpha) \qquad (19)$$

$\phi_{(r_\alpha)}^\alpha = \sum_{lm} R_{nl} R_{nl}^\alpha(\theta, \varphi)$ where $R_{nl}^\alpha(r)$ and $Y_{lm}(\theta, \varphi)$ are respectively radial and the angular portions. The ϕ_j^α are the atomic orbitals (called also atomic basis functions) and the C_{ij}^α the MO expansion coefficients.

In DMol3 the user is given an option to choose a basis set between MIN (minimal basis), DND (double numerical plus d-function, DNP (double numerical plus polarization) or the TNP (triple numerical plus polarization). The choice of the basis set should be guided by the physics of the problem and the cost of calculations. In our calculations we used the DND basis.

2.6.3 Orbital Cutoff

In the expression of the Bloch Theorem,

$$\Psi_i(\mathbf{r}) = u_k(\mathbf{r} + \mathbf{T})\exp(i\mathbf{k}.\mathbf{r})$$

In the reciprocal space, it can be written as

$$\psi_{ik}(\mathbf{r}) = \frac{1}{\sqrt{\Omega}} \sum_G c_{ik}(\mathbf{G}) e^{i(\mathbf{K}+\mathbf{G})\mathbf{r}}$$

The set of reciprocal lattice vectors G for which this expression is verified is infinite; that means that the calculation over the set of these vectors may last forever if we do not set a certain limit. In a realistic system the orbital plane waves become negligible for large values of G vectors. That allows us to limit our calculations in certain radius around the nucleus. The cutoff specifies the finite range of the basis set. In our calculations we mostly used a radius cutoff of about 4.400 Angstrom.

2.6.4 Core Treatment

The core treatment is used to specify how the core and valence electrons should be included in your calculations. In the DFT, all-electron methods treat core and valence electrons on an equal level, but the pseudopotential methods treat cores electrons as frozen such that they are not included in chemical bonding. In our calculations we had an option to choose between: all electrons, effective core potentials, all Electron relativistic and DFT semi-core pseudo-potentials. In this work we used the all electron option.

Chapter 3

Clean Surfaces

3.1 Introduction

In this work a clean surface is any of the surfaces Cu(100), Cu(110) or Cu(111) that has no impurities. In order to understand the properties of clean surfaces and adsorbed surfaces it is important to understand how the copper atoms are arranged inside the bulk material. From the solid state course we know that in ideal crystal atoms are arranged in a 3D periodical lattice which is defined by three translation vectors **a**, **b**, **c** (in this part we are going to use the bold font to indicate that the letter represents a vector). Any point in the crystal can be described in the form R = n**a**+m**b**+k**c** where n, m and k are integers and **a**, **b**, **c** are the primitive vectors. In the case of copper a= b= c, and the conventional unit cell is a Face Centered Cubic (FCC). Therefore the copper lattice is characterized by its lattice constant which is the length of the side of the conventional cell. It is experimental value is 3.6147 Å.

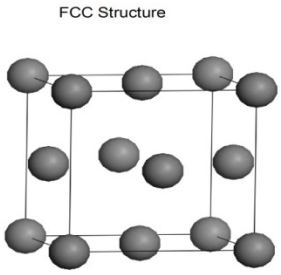

Figure 3-1 FCC structure

Since the experimental value is sometimes different from the calculated one, it was important that we verify that the copper bulk constant used in this work is the right one[04,05]. For this purpose we referred to works done by other who used the same code as the one used in this work.

Theoretically the lattice constant can be calculated using the Murnaghan equation of state and by fitting the data to this equation.

$$E = E_T + \frac{B_0 V}{B_0'}\left[\frac{(V_0/V)^{B_0'}}{B_0'-1} + 1\right] - \frac{V_0 B_0}{B_0' - 1} \qquad (20)$$

where V is the volume, B_0 and B_0' are the bulk modulus and its pressure derivative at the equilibrium volume V_0 . Those parameters allow to plot the energy (E) vs unit cell volume (V) data. In this work we did not calculate the bulk constants, and Willie Burton Maddox [04] calculated the lattice constant and found the value of 3.64 Å. X.Duan and the team [05] found the same value using the DMol3 code. This value is in good agreement with the experimental value of 3.615 Å. It is important to mention that even though the experimental value is

different from the calculated value, we preferred to use the calculated value in this work since it is the value calculated by the same code. We used the calculated value as reference in the study of surface relaxation and adsorption. The interlayer spacing of the relaxed and adsorbed surface will be calculated relative to that value.

3.2 Miller indexes

In the clean bulk Cu atoms are arranged in array of points and distributed in set of parallel planes called Miller planes. Miller planes refer to sets of parallel planes defined by a set of Miller indices (h k l), where h, k, and l are integers. These planes are defined (using fractional coordinates x, y, and z) by the equation: $hx + ky + lz = m$ where m is an integer

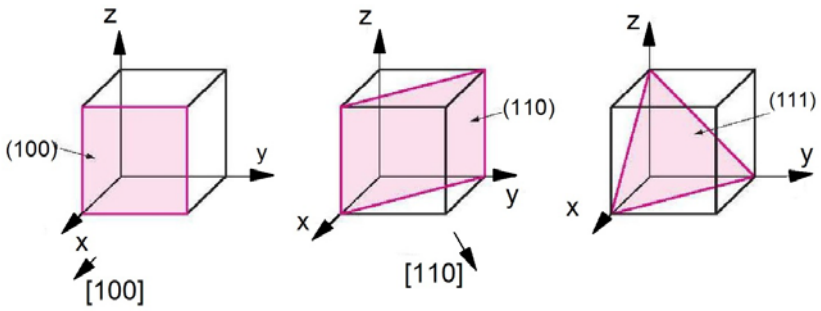

Figure 3-2 Miller indexes

Any lattice point in the crystal can be placed in any of those planes. All planes of this form pass through periodical lattice points.

The plane corresponding to the integer m has intercepts of m/h, m/k, and m/l respectively with the ox, oy and oz. A value of 0 for h, k, or l indicates that the plane is parallel to that axis. The family planes with Miller indices (h k l) can be translated to pass through any point in the crystal lattice. The atomic arrangement and atomic layers spacing depend on the miller index of the surface in study. Through any point of the crystal we can draw Cu(100), Cu(110) or Cu(111) surface, and the electronic properties of the surface depend on the miller index of the surface we consider.

3.3 Unit Cells

The unit cells used in our calculations are shown in the Fig 3.3. The shape and the dimensions of the unit cell depend on the miller index and the user. A same surface can be represented by different unit cells. In this work we considered the smallest unit cell that we can have for each surface. With these unit cells neighborhoods of all points are identical under translation. The R position of any point on the surface is described by two vectors u and v such that

$$\mathbf{R} = n_1\mathbf{u} + n_2\mathbf{v}$$

where u and v are the primitive or cell vectors. If $n_1 = n_2$=1, we have a unit cell. The unit cell is the smallest entity from which we can generate all the points on the surface. We use the term surpercell to designate any cell obtained from the unit cell by rotating or multiplying the length of the sides of the unit cell. It is also important to mention that all direction will be given in reference to FCC

conventional cell axis, therefore the x-axis direction will refer to the [100], the y-axis to [010] and the z-axis to [001] as shown in the figure 3.2

In the figure 2.3, the Cu (100) surface is characterized by a square primitive surface mesh which is rotated 45 degrees with respect to the conventional FCC unit cell. The Cu (110) is characterized by rectangular primitive surface mesh whose one of the unit vectors is parallel to [001] direction and the other along a face diagonal, which is along [110] direction. The Cu (111) surface is represented by a hexagonal primitive cell. The cell vectors of the Cu (111) form a 120 degrees angle.

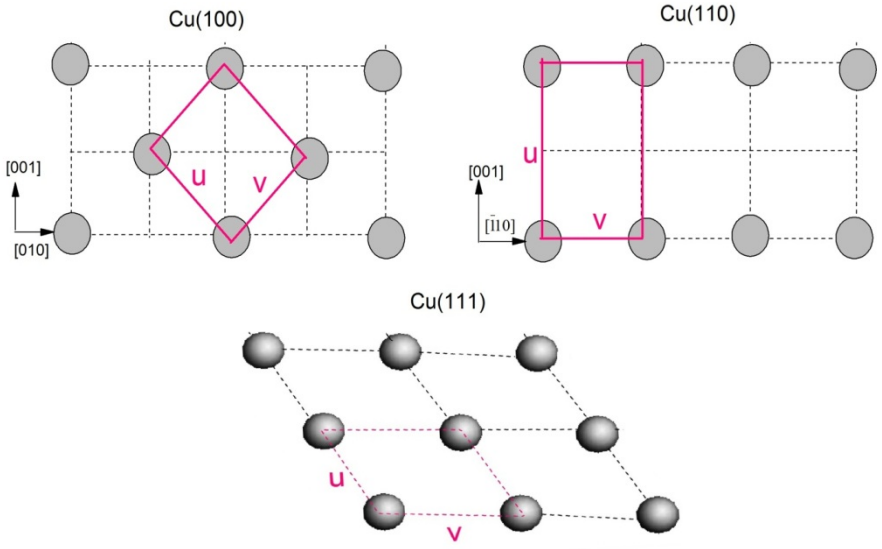

Figure 3-3 Unit Cells for Cu(100), Cu(110) and Cu(111)

The unit cell of Cu (100) is a square with side u=v=2.556Å; it is rectangle with sides of u=3.615 Å and v=2.556 Å for Cu (110); and it is hexagon with side of u=v=2.556 Å for Cu(111).

3.4 Interlayer Spacing

DMol3 calculations can be done only for 3D structures. Therefore in order to study the atomic relaxation of any structure, a vacuum region should be added to make the structure periodic in space. A third coordinate is added in the direction perpendicular to the atomic slab and along the vacuum slab. In this work, we will used (u, v, w) system of coordinates where u and v are in the atomic plane and w in the direction normal to that plan, which is also parallel to the vacuum slab. In the coordinates files, x, y, and z are used respectively in the place of u, v, and w. An example of a coordinates files used by DMol3 is given in the Fig A.2 in the appendix. In this table the last column of numbers represents the z coordinates which are measured in the direction normal to the atomic slab.

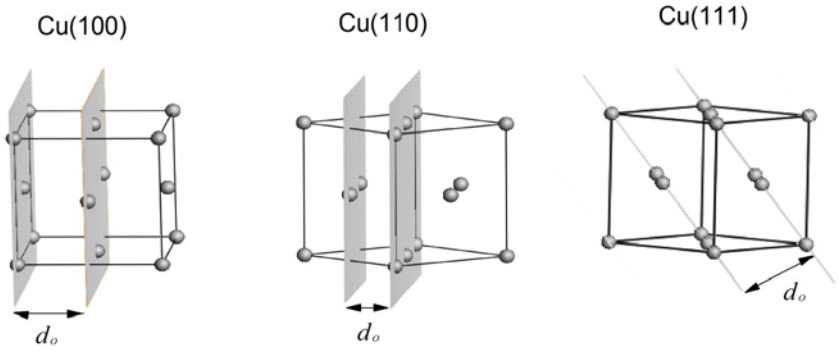

Figure 3-4 Interlayer Spacing

The figure show the interlayer spacing in the bulk for Cu (100), Cu(110) and Cu(111). d_o is 1.807 Å for Cu(100), 1.278 Å for Cu(110), and 2.87 Å for Cu(111)

The arrangement of copper atoms in the super cell for each surface is shown in the figure 3.5. In our slab model calculation the top and the bottom layer should be symmetrically the same, so it is the same unit cell that describes the positions of atoms in the top and bottom layers.

In the ideal crystal the planes with the same miller indexes are separated by a constant distance that we call here interlayer spacing. The interlayer spacing is an important notion in the study of relaxation and adsorption on the surfaces. This distance changes with the oxygen coverage. For clean surfaces, considering the experimental value of 3.615 Å for the copper lattice constant, two consecutive Cu (100) atomic layers are separated by a distance of 1.807 Å. For the Cu (110) and Cu (111) surfaces this distance is respectively 1.278 Å.and 2.87 Å.

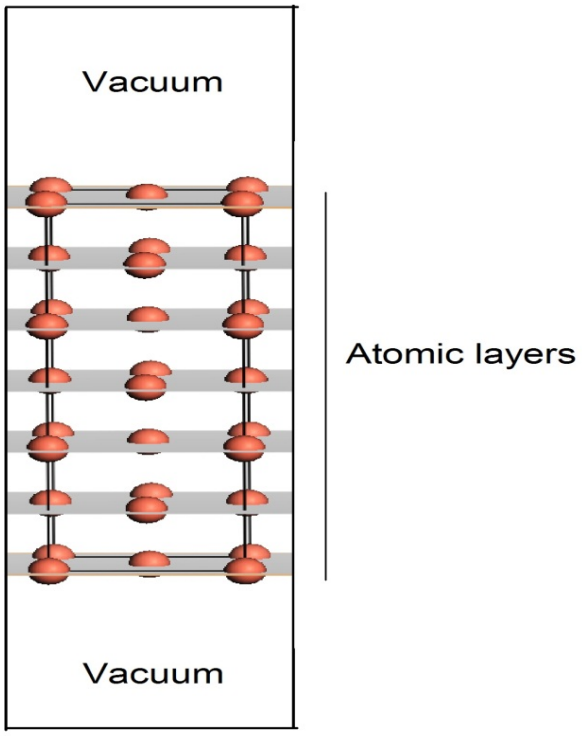

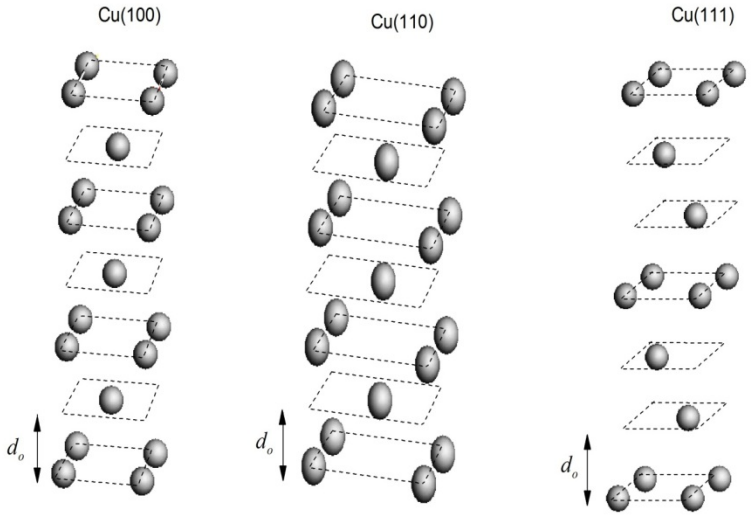

Figure 3-5 Computational supercells for Cu(100), Cu(110) and Cu(111)

The figures 3.4 and 3.5 show how those distances are calculated. The table in the figure A.2 in the appendix show the example of coordinates files used to do DMol3 calculations. In this table atoms that have the same z coordinates(the third column of numbers) belong to the same atomic layer, and the interlayer spacing between two atomic layers is just the difference of their z coordinates. Since we deal with realistic structures, in our calculations we used the calculated value of 3.64 Å [04, 05].

3.5 Slabs Preparation and Method Used

Because of the Bloch's theorem we can study the electron structure of an infinite solid by considering just an elementary cell of this solid. To study a surface we consider a 3D period cell formed by atomic slabs surrounded by vacuum regions on the top and bottom. Fig 3.5 shows such a super cell. In this approach the surface in the study is placed on the top and bottom of the atomic slab since it is the one that is in contact with the vacuum. The symmetry should also be taken into consideration so that the bottom and the top layers represent the same surface. To efficiently represent a real material, studies show that the number of atomic layers and the vacuum slabs must be large enough. It is shown that for a number N of atomic layers less than 6 the total energy is not stable. The same conclusion is confirmed for vacuum width less than 20 Å. In this work in order to reduce the computational time, we adopted the number of atomic layers to be 7 (or 9 in some cases) and a vacuum slab of 30 Å.

Since we are studying the behavior of a real surface surrounded by vacuum, the layers below the vacuum slab should resemble the layers of real crystal. It is shown that only the atomic layers close to the vacuum region are affected by the relaxation [04,05]. For this reason to mimic the behavior of the atoms inside the bulk, we kept the fourth atomic layer fixed at its bulk but let three layers below the vacuum region free to relax. The change to the interlayer spacing is evaluated relative to the position of the fixed layer. In this work we imposed constraints to the atoms so that the atoms in the middle of the slab keep their bulk positions. In some cases of reconstructed surfaces where there is a need for large super cell in calculations we had to use super cells with five atomic layers to reduce the time of calculation. But in this case, the surface in study was placed on one side of the atomic surface layer and the atoms on the opposite side of slab were fixed their bulk positions.

Regarding other parameters, in this work all calculations were done using the DFT as implemented in the DMol3 software. The input files were generated or constructed manually with the help of the Material Studio interface. We used the GGA approximation for functional, the DND basis and real cut-off of 4.5 Å.

After building the super cell for calculations, some parameters need to be set for the accuracy of the result. The figure 3-6 shows the different choices we have for the potential, the wave function, the exchange-correlation potential. In this work we used the GGA approximation for exchange-correlation potential, all

electron full potential, and the numerical LCAO for wave function basis. Other parameters that need to be set for the accuracy of the calculations are shown in the table in the figure in appendix part.

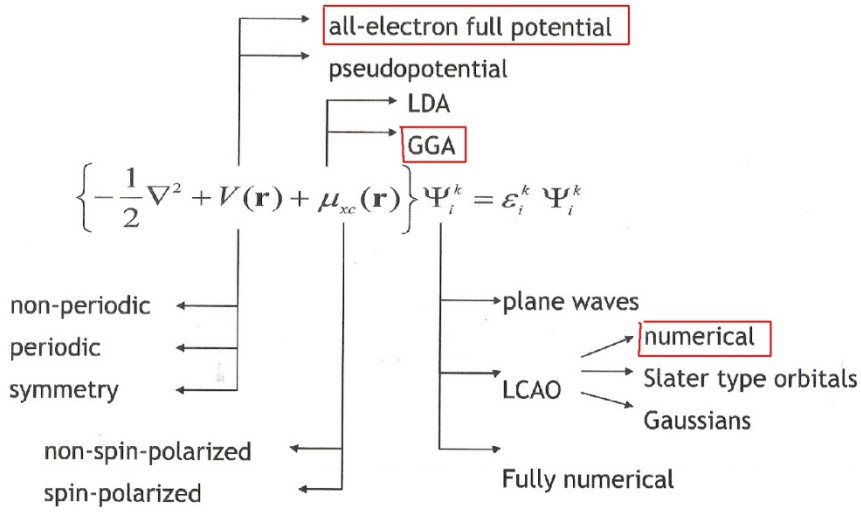

Figure 3-6 Computational choices

3.6 Relaxation

When a metal surface is exposed to vacuum, two phenomena may occur to the atoms at and near the surface: the relaxation and the reconstruction. In other words, if (x,y,z) are the cartesian coordinates of an atom on the surface, after the relaxation the new coordinates become (x',y',z') with x=x', y=y' and z≠ z'. z and z' are coordinates along the axis normal to the surface. The relaxation is a rearrangement of the top most atomic layers in the direction normal to the surface.

In this process, the spacing between atomic layers near the vacuum surface contract or expand compared to the normal spacing in the bulk. After a relaxation process the distances between atoms in the same surface remain unchanged, but the interlayer distance contract or expand depending on environment above the surface. In the relaxation process the atoms of the entire atomic layer move in the normal direction to the surface.

The reconstruction on the other hand involves not only a change in spacing between atomic layers but also a change in distances between atoms of the same layer. The reconstruction involves the modification of the orientation and the lengths of the super cell vectors. If (x ,y, y) are the coordinates of an atom, after the reconstruction they become (x', y, z') with x≠x, y≠y' and z≠z'. A reconstruction can be characterized by a number and an angle. For instance after a $(\sqrt{2}, 2\sqrt{2})$R 45° missing reconstruction the two vectors (a, b) of the surface unit cell are changed in such way that the new vectors are obtained from the original ones by rotating them by 45°and multiplying them respectively by $\sqrt{2}$ and $2\sqrt{2}$. That means that the new unit cell will be (a$\sqrt{2}$, b$2\sqrt{2}$) and rotated by 45°from their original position.

The cause of relaxation and reconstruction can be explained by the breaking of the equilibrium of forces between atoms. The net force on the atoms near the surface is not the same as for the atoms in the deeper layers.

In this work we studied the relaxation of the Cu(100), Cu(110) and Cu(111) surfaces using the slab method. In this method we simulate the situation where the surface of an infinite crystal surrounded by the vacuum region on the top is subjected only to the atoms inside the bulk. We relaxed the surfaces and calculated the interlayer spacing of the three top layers of each surfaces. Then we computed the other electronic properties of the relaxed surface.

We found that the interlayer distances between the first three layers exposed to vacuum changed after relaxation. The calculated relaxation parameters are in the table 3-1, 3-2 and 3-3. In these table the Δ_{ij} represent the percent change in the interlayer spacing between the ith and jth layers. $\Delta_{ij}= 100(dij/d_0 - 1)$ where dij is the interlayer spacing after relaxation and d_0 is the interlayer spacing in the ideal bulk (1.82 Å for Cu(100), 1.30 Å for Cu(110) and 2.10 Å for Cu(111).

Table 3-1 Relaxation data for clean Cu (100)

	$\Delta_{12}(\%)$	$\Delta_{23}(\%)$	$\Delta_{34}(\%)$
This work (TW)	-2.0	+1.1	+0.4
Ref[04]	-1.7	+0.82	+0.49
Ref[05]	-2.3	+1.0	
Exp (LEED)[10,11]	-2.1	0.5	
Flapw	-3.02	+0.08	-0.24
Ref[09] DFT-GGA	-2.6	+0.99	

Table 3-2 Relaxation data for clean Cu (110)

	$\Delta_{12}(\%)$	$\Delta_{23}(\%)$	$\Delta_{34}(\%)$
This work (TW)	-9.4	+4.6	-1.50
Ref[04]	-8.41	+2.84	-1.18
Ref[05]	-10.0	+3.0	
Exp[12]	-10.0	+2.5	$\mp$2.5
Flapw[13]	-9.7	+3.6	
Ref[09] DFT-GGA			
Ref[10] LEED			

Table 3-3 Relaxation data for clean Cu (111)

	$\Delta_{12}(\%)$	$\Delta_{23}(\%)$	$\Delta_{34}(\%)$
This work (TW)	-0.41	-0.28	-0.10
Ref[04]	-0.39	-0.33	-0.17
Ref[14]	-0.9	-0.3	
Exp[15,16]	-0.7	-0.3	

If follows from the results obtained in this work that the three surfaces do not relax in the same way. The positive sign for Δ_{ij} corresponds to an expansion and the negative sign to an expansion. Comparing our values to the experimental

values and other reported values, it can be seen that our values are in good agreement with experimental and other reported results. It can also be seen that for the Cu(111) all the first three layers contract, and for Cu(100) the first layer contracts and the two other layers expand, and for the Cu(110) the first and the third layers contract while the second layer expand.

3.7 Work Functions for Clean Surfaces

The work function is defined as the minimum energy required to extract an electron from the crystal to a point at infinity. This quantity depends on crystal structure and the orientation of the surface.

In this work, we used the slab approach to calculate the work function for the Cu(100), Cu(110) and Cu(111) surface. In this approach, if the vacuum slab is large enough, the potential energy in the middle of the vacuum slab will be approximated to be zero. This approach allows us to calculate the work function as the difference between the Fermi energy and the electrostatic potential in the middle of the vacuum slab from the surface.

$$\phi = V_{\infty} - E_F$$

where E_F is the Fermi energy and V_{∞} the potential energy in the middle of the vacuum slab. It is important to mention that, here, the Fermi energy is calculated relative to the crystal zero.

The DMol3 output provides the Fermi energy and the spatial distribution of the electrostatic potential (averaged values) along the normal to the surface

layers. Those averaged values are used to plot the electrostatic potential inside the vacuum and the atomic slabs. The work function is the difference between the Fermi energy and the potential in the middle of the vacuum slab. If the vacuum slab is large enough, the value of the potential in its middle is zero. In this case the work function is simply be the Fermi energy.

The Figure 3.7 shows the averaged potential along the axis normal to the surface atomic layers for Cu (100). The same method was used to compute also the average potential and the work function for Cu (110) and Cu (111) .The results of our calculations are shown in the table 4.2

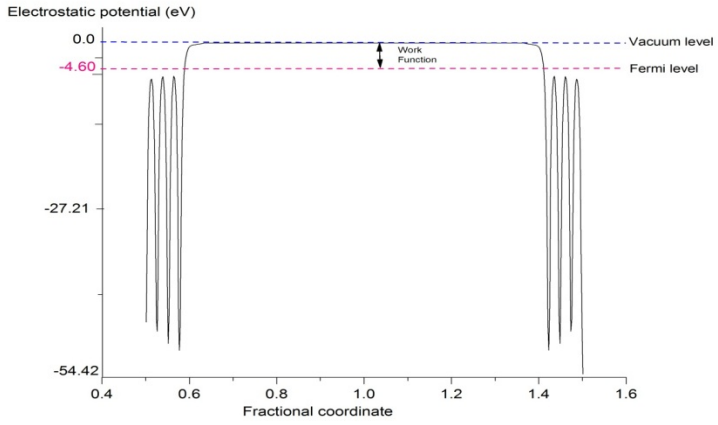

Figure 3-7 Average potential along z-axis and work Function

This figure shows how the electrostatic potential behaves inside the atomic the vacuum slabs. It fluctuates inside the atomic slab and stays constant in the vacuum slab.

Table 3-4 Work Function for clean surfaces

	Cu(100) (eV)	Cu(110) (eV)	Cu(111) (eV)
This work (TW)	4.60	4.29	4.80
Ref[04]	4.49	4.26	4.77
Ref[05]	4.59	4.18	
Ref[18](exper.)	4.59	4.48	
Ref[19] (theor.)	5.26	4.48	
Re[14]			4.78

It follows from this table that the work function is not the same for all the three surfaces. The Cu(111) has the largest value followed by Cu(100) and Cu(110). That shows that the work function depends on the surface orientation and the density of atoms at the surface. Considering their unit cells, the Cu(111) is the most dense followed by Cu(100) and Cu(110).

Our calculated values were compared to experimental and theoretical values, and it can be seen that there is a good agreement between them.

3.8 Density of States of the Clean Surfaces

The density of states (DOS) is used to characterize the electronic structure of a material by counting the number of energy levels in each energy range. Therefore it has the value of 1 at the energy eigenvalues and zero elsewhere

Mathematically for a given band n, it is defined as

$$N_n(E) = \frac{1}{4\pi^3}\int \delta\big(E - E_n(k)\big)\, dk$$

$E_n(k)$ is the dispersion of the band and the integral is calculated over the BZ. The total number of electrons in the unit cell.

$$N=\int_{-\infty}^{E_F} N_n(E)\, dE$$

The partial density of states gives the DOS in terms of contributions from particular atomic orbitals. The figure 3.8 shows the plots of total DOS and PDOS for Cu (110).

In this work we computed the total DOS for the three low index surfaces of the copper and the results are in the figures bellow

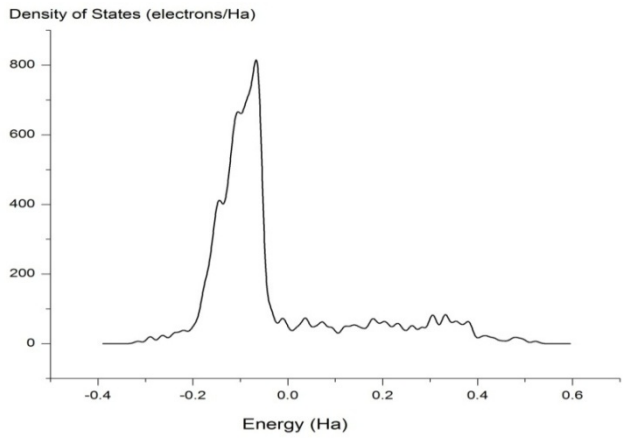

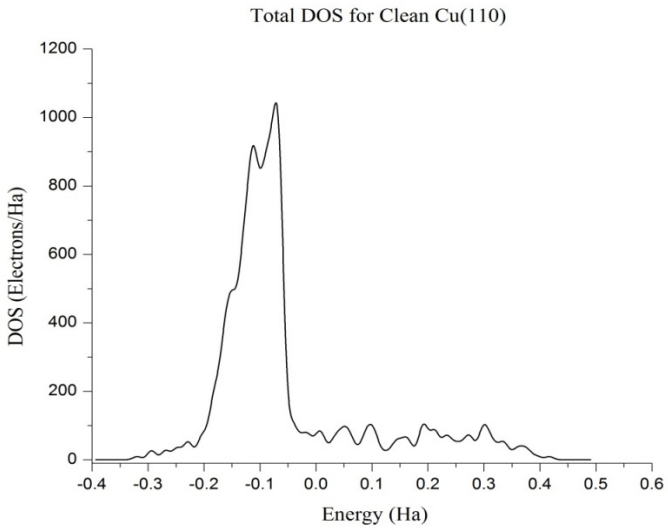

Figure 3-8 Densities of states for clean surfaces

Chapter 4

Oxygen Adsorption on Cu (100)

4.1 introduction

Many studies have been conducted on the oxygen adsorption of oxygen on the Cu(100) surface, and they have confirmed that at coverage of 0.5ML or above 0.5ML the Cu(100) surface undergoes the so called “missing row”. The low energy electron diffraction (LEED), the x-ray diffraction (XRD), as well the scanning tunneling microscopy have provided large information on the formation of this reconstruction. In this part of our work we will present the results of our studies on the effect of the missing row reconstruction on the electronic properties of the oxidized Cu(100) surface. The focus was put mostly on the changes of the interlayer spacing, the work function, and density of states. We used the same method as the one used in the study of clean surface.

Two types of structures were considered in this work: the non-reconstructed structure, and the missing row structure. In the non-reconstructed structure, the supercell keeps the same form and dimensions as for the clean surface, and for the missing row the super cell is modified as explained in the part 4.3 of this chapter.

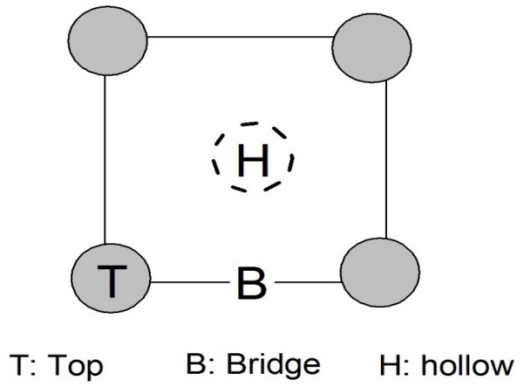

Figure 4-1 On-surface adsorption Sites for Cu(100)

Before we present our results on the studies of the adsorption of oxygen on the Cu(100) surface, it is important that we explain some terms that are used in the two last chapters of this work.

The adsorption is the penetration of foreign atoms into a solid surface. From that definition, the substrate is the material of the host surface and the adsorbate is an added substance. For example, in the case of oxygen adsorption on Cu (100) surface, the Copper is the substrate and the oxygen is the adsorbate. The concentration of the adsorbate on the substrate surface is characterized by its coverage. The coverage is expressed in terms of monolayer. One monolayer corresponds to one adsorbate atom for each unit cell surface of the ideal non - reconstructed substrate surface. In the case of the adsorption of oxygen on Cu (100) surface, since there is one atom per unit cell, the coverage is simply the number of oxygen adatoms per number of Cu atoms in the super cell. In the case

when the oxygen atom occupy also the sub surfaces, the coverage is calculated relative to the top surface and the calculations are done by adding the number of sub adsorbate atoms to the total number of atoms on the top surface.

Regarding the question where an oxygen atom should be placed in the super cell, there are three adsorption sites in Cu (100) unit cell. The top site is located directly above a copper atom in the topmost layer, the hollow site is a fourfold site located in the center of the square formed by four surface copper atoms, and the bridge site is located at the mid-point between two copper atoms on the same side of the unit cell square. It is also important to mention that, in the case of on-surface adsorption, an adatom should be placed at about one Angstrom above the surface so that during relaxation the adatom will find an equilibrium position. The figure (4.1) shows the location of the on-surface adsorption sites.

In some cases, the oxygen atoms would prefer to go underneath the top atomic layer. In this case we say that this oxygen occupies a sub-surface site. There are two sub surface sites for Cu (100), the octahedral site and the tetrahedral site. The octahedral site is located in the second layer and directly under a copper atom, and the tetrahedral site is located at the bridge site but between the top layer and the second layer. Kangas and Lasson examined in details the combination of the on-surface and sub-surfaces sites [28]. In this work we considered only the case of on-surface adsorption.

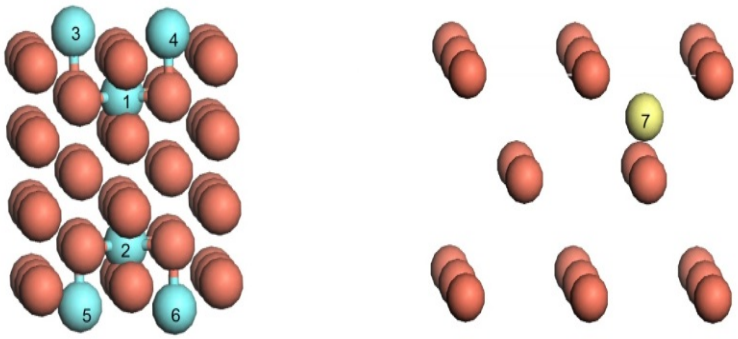

Figure 4-2 Octahedral and Tetrahedral Sites

In this figure, the atoms 1 and 2 are occupying octahedral sites and the the atom 7 a tetrahedral site.

The same method used for clean surface was also used to study both the non-reconstructed and the reconstructed structures, but before adding the oxygen adatoms, the structures were built and then relaxed. The oxygen atoms were placed at hollow sites, and at approximately one Angstrom above the surface.

4.2 Non Reconstructed Cu(100)

We studied this structure for coverage of 0.11ML, 0.25ML, 0.5ML 0.75ML and 1.0ML. In this Part of our work all the super cells were built from the (1x1) unit cell described in the previous chapter, and they are shown in the figure 4-3.

To study the stability of the structure when the oxygen atoms occupy a particular adsorption site, we considered the (2x2) super cell and we alternately

placed an oxygen atom at the top site, hollow site and bridge site. The result of our wok is shown in the Table 4.1. The values of energy in this table are calculated in respect to the crystal zero energy.

It can be seen that the structure with the oxygen atom at the hollow site has the least value of the total energy, and the structure with the oxygen atom at the top site presents the greatest value. That confirmed claim that the hollow site is the most favorable site for oxygen adsorption on Cu(100) surface, see also Ref [05, 28]. Therefore, in this part of our work, the oxygen adatoms were placed at hollow sites.

Table 4-1 Total energy for different adsorption sites

Sites	Total Energy
Bridge	-6395.0838 Ha
Hollow	-6395.3100Ha
Top	-6390.2537

The 0.11ML, 0.25ML, 0.5ML, 0.75ML and the 1ML coverages were studied using respectively (3x3), (2x2), (2x2) and (1x1) supercells. The figure (4.3) shows the supercells used to study the 0.25ML, 0.5ML, 0.75ML and 1.0ML. The coverage is calculated by dividing the number of oxygen atoms by the number of copper atoms in the supercell.

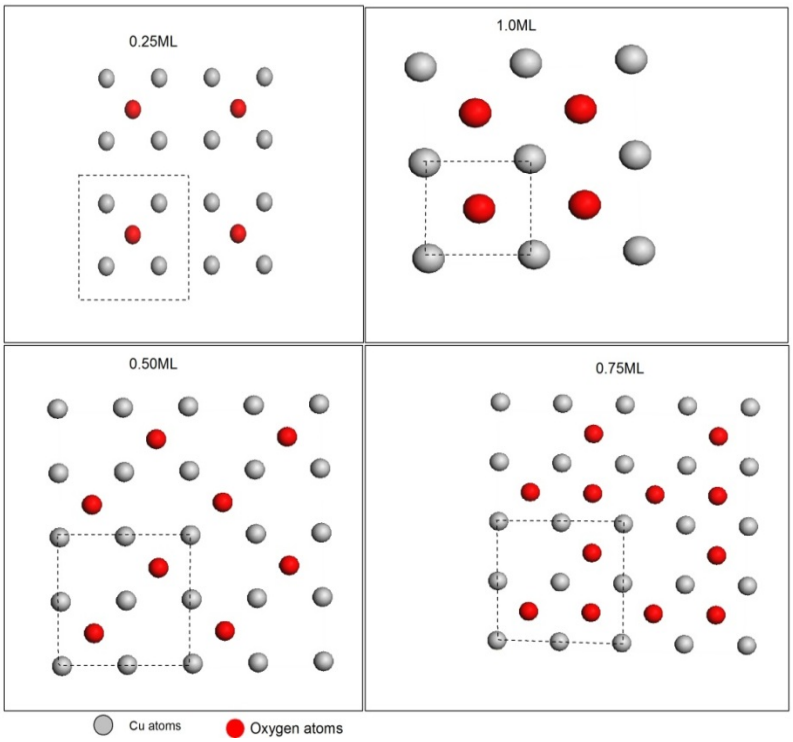

Figure 4-3 Supercells used for different coverages

This figure shows the supercells used for the study of 0.25ML, 0.50ML, 0.75ML and 1.0 ML. The red colored spheres represent the oxygen atoms and the grey ones the Cu atoms in the top layer.

Our calculated values for the relaxation O/Cu(100) are shown in the table (3.2). Our results show that, as the oxygen coverage increases from 0.1ML to 1ML, the minimum distance d_0 (height) between the O atoms and the Cu atoms in the top layer decreases, and the average of the length bonds between Cu atoms and O remains does not change munch.

Table 4-2 Relaxation data for O/Cu (100)

		d_0(Å)	d_{Cu-O}(Å)	Δ_{12}(%)	Δ_{23}(%)	Δ_{34}(%)
0.11ML	TW	0.8	2.0	+0.50	+0.7	+1.0
	Ref[04]	0.794	2.011	+0.055	-0.55	0
	Ref[05]	0.81	2.081	+1.1	+0.5	+0.6
0.5ML	TW	0.8	2.0	+0.5	+0.4	+0.5
	Ref[04]	0.822	2.0	+0.89	-1.8	+0.49
	Ref[05]	0.82	2.01	+0.6	+0.4	+0.6
0.75ML	TW	0.6	2.0	+14.3	+0.5	+0.4
	Ref[05]	0.68	1.95	+14.3	+0.6	+6.0
1.0ML	TW	0.6	1.80	+18.7	-1.0	1.0
	Ref[05]	0.51	1.89	+18.7	-1.7	+1.1

It can also be seen that our results are good agreement with other reported results [04, 05]. It is important to mention that here the percent change of the interlayer spacing is calculated using the formula Δ_{ij}= 100(dij/d_{ij}^{rel}- 1) where d_{ij}^{rel} is obtained from the relaxation of the clean surface, and dij is the average of the interlayer spacing between ith and jth layers in the adsorbed structure.

4.2.1 Work Function

We also calculated the work function using the same method we used for the clean surfaces. Our results are given the following table.

Table 4-3 Work function change with coverage for Cu (100)

Work Function (eV)						
	0ML (clean)	0.11ML	0.25ML	0.5ML	0.75ML	1.0ML
TW	4.29 eV	4.70 eV	4.85 eV	5.10 eV	5.50 eV	5.75 eV
Ref[04]	4.49 eV	4.80 eV	5.19 eV	5.44 eV		
Work Function Change (eV)						
TW		0.41 eV	0.56 eV	0.81 eV	1.21 eV	1.46 eV
Ref[05]		0.4 eV	0.7 eV	0.9 eV	1.3 eV	1.5 eV

It can be seen from these data that the work function change increases with coverage. This can be explained by the fact that when the coverage increases the effective negative charge due to oxygen atoms also increases. This accumulation of negative charges makes difficult for an electron to be removed from the surface.

The following figure show how the work function changes with the oxygen coverage.

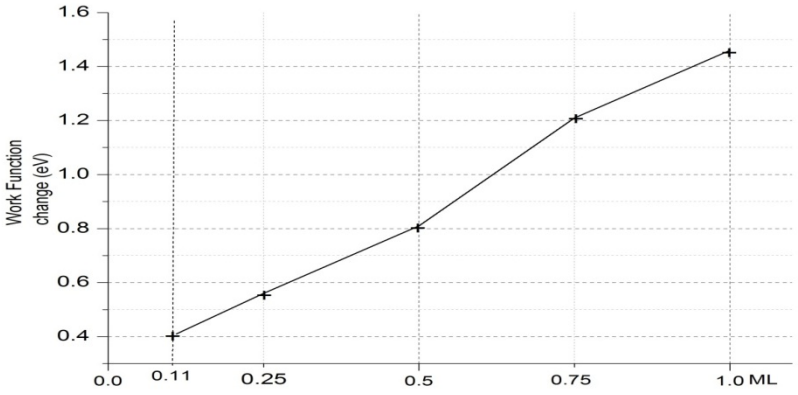

Figure 4-4 Work function Change for differrent coverages

4.3 Missing Row

As we mentioned before, a high oxygen coverage induces the so called "Missing row" on the Cu(100) surface. In this part of our work we studied the the interlayer spacing and work function of a Cu(100) missing row reconstructed surface.

In this work, we focused our study only on the $(\sqrt{2}, 2\sqrt{2})$R 45° and $(2\sqrt{2}, 2\sqrt{2})$R 45° supercells which correspond respectively to 0.5ML and 0.25ML.

The $(\sqrt{2}, 2\sqrt{2})$R45° supercell is obtained from the 1x1 unit cell by rotating both lattice vectors about 45°, multiplying them respectively by $\sqrt{2}$ and $\sqrt{2}$, and deleting an entire row as shown in the Fig (4.5) The figure (4.6) show the top and side views of the $(\sqrt{2}, 2\sqrt{2})$R 45° Missing Row super cell.

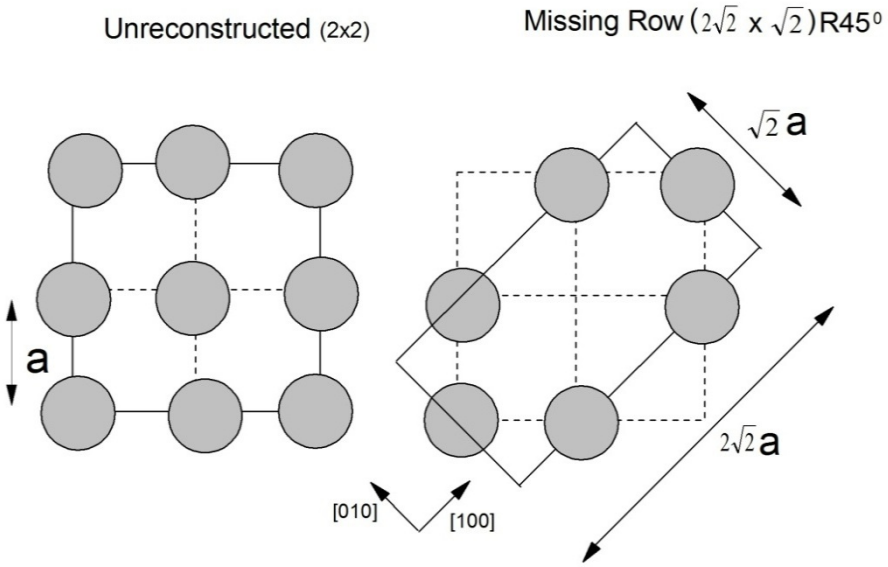

Figure 4-5 Formation of Missing Row

In our slab method, the MR reconstruction affects only the atoms of the layer exposed to the vacuum, so only the top and the bottom layers of the 7 layers are modified, the other layers keep their structure as in the 0.5 ML and (2x2) super cell studied in the previous part.

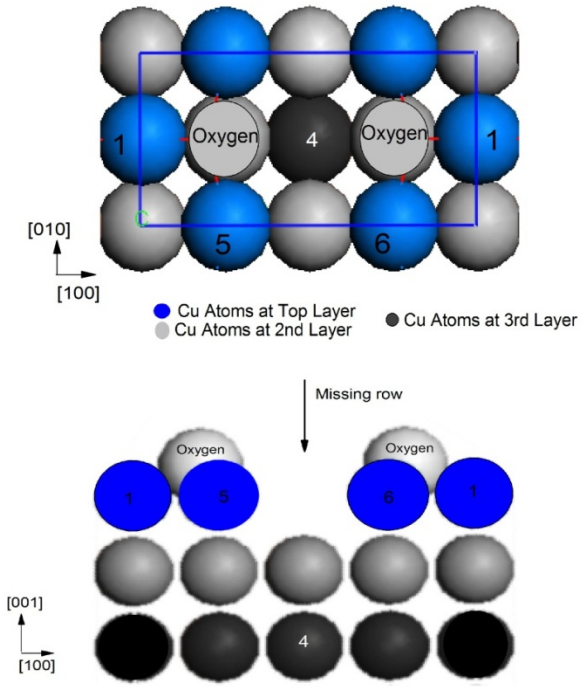

Figure 4-6 Top View and Side View of Missing Row Supercell

Our calculated values for the relaxation on the missing row structures are shown in the table 4.4.

Table 4-4 Relaxation data for Missing Row

		d_0(Å)	d_{Cu-O}(Å)	Δ_{12}(%)	Δ_{23}(%)	Δ_{34}(%)
0.25ML	TW	0.1	2.0	+4.0	+1.9	+1.0
	Ref[05]	1.13	1.86	+6.0	+2.2	+0.6
0.5ML	TW	0.1	2.0	+3.0	+2.0	+0.4
	Ref[05]	0.18	1.86	+4.4	+2.2	+1.1

Our results are in good agreement with the results of ref [05] that have been calculated with the same method and code. It can all the three layers are expanded after the laxation of the structures.

Chapter 5

Oxygen Adsorption On Cu (110)

5.1 Introduction

Similarly to the Cu(100), many studies show that the Cu(110) surface can undergo reconstruction due to oxygen coverage. Chemisorption studies prove the formation of reconstructed Cu(110) surface. It has been known that 0.5 ML oxygen coverage can induce a (2X1) reconstruction, but the mechanism and the position where the oxygen atom s should occupy remains subject of debate for long time. Now STEM data have confirmed a missing row type reconstruction called “Added-row” because of the mechanism of formation leading to this reconstruction. The added row reconstruction is generally admitted, and all studies agree that oxygen is located in the long bridge site between two neighbor copper atoms. The case where the oxygen atoms occupy the short bridge site is also possible, but it seems to be unstable [05]. We have examined this case and found that the oxygen atoms at short bridge cause the first copper layers to expand irregularly. Therefore we focused on the reconstructed structure where the oxygen atoms occupy the long bridge positions forming a (2x1) structure.

Even though the reconstruction can occurs before the full coverage, we examined also the case of non-reconstructed surface where we considered the coverage 0.25ML, 0.50 ML, 0.75ML and 1.0ML. For the unreconstructed surface

we also calculated the work function change for oxygen coverage going from 0.25ML to 1.0ML.

5.2 Non reconstructed surface

5.2.1 Adsorption Sites

In this work we have studied the oxygen adsorption on Cu(110) by considering the Non reconstructed and the reconstructed Structures, and we are more interested in the on surface sites. The Non reconstructed Cu(110) surface presents five available sites for oxygen adsorption: The hollow site, the long bridge site, the short bridge site, and the shifted-hollow site. The fig(5.1) show the location of each site.

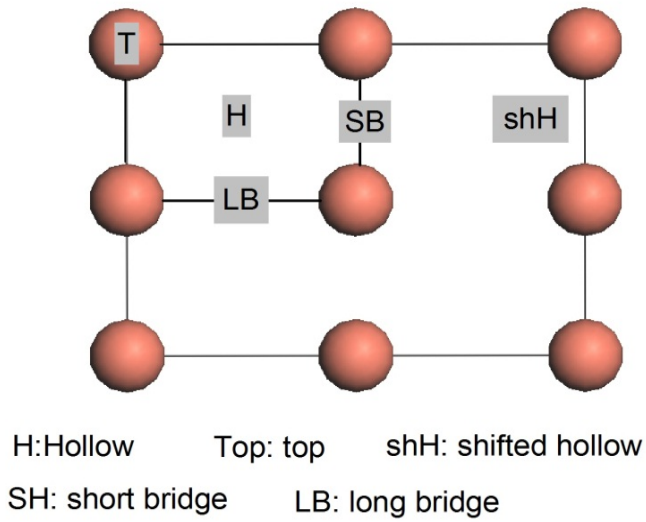

Figure 5-1 On-surface Adsorption Sites for Cu(110)

The oxygen adatom located at hollow site is surrounded by four Cu atoms of the same layer, an oxygen atom located at the long-bridge site is located at the midpoint between two Cu surface atoms lying along the [001] direction, the short bridge oxygen adatom is located at midpoint of two surface Cu atoms lying in the [110] direction, and the top adatom is located directly above a Cu atom. In our simulation, for all the four adsorption sites, the oxygen adatom was placed at 0.9 Angstrons above the surface we are studying. As for Cu(100) the top site is proved to be the most unstable. Contrary to the Cu(100) surface where the hollow site is considered the most stable, for the Cu(110) surface, at low coverage, the shifted hollow site is considered the most stable followed by the hollow site, the long bridge and the short bridge [05]. At the coverage of 0.5ML, the structure with the an atom at long-bridge become more stable than the one with an atom at the hollow site, and at the coverage of 1/3 ML the long bridge become the most stable position for the oxygen adsorbed atom[05]. After all, when the reconstruction has been induced the oxygen atoms will occupy the long-bridge sites and will form Cu-O-O chains with the oxygen atoms.

To know which site is favorable for oxygen adsorption we switched around the O atom at different adsorption sites of the (2x2) super cell. The oxygen adatom was placed alternately at hollow, long-bridge, short bridge and shifted hollow site. Our results which are in the table 5-1 confirmed that the shifted-hollow site is the most favorable because it presented the lowest total

energy. In this work, for simplicity reason, we used the hollow site as adsorption site since there is no significant difference between the energy of the structure with oxygen at hollow site and the one with oxygen atom at shifted-hollow site.

Table 5-1 Total energy for different Sites of Cu (110)

Sites	Total Energy
Short bridge	-32966.486 Ha
Long bridge	-32966.483 Ha
Hollow site	-32966.619 Ha
Shifted-hollow site	-323966.638 Ha

5.2.1 Relaxation

To study the effect of oxygen adsorption on the non-constructed surface on the interlayer spacing, for the coverage going from 0.25ML to 1.ML, we used the (2x2) super cell. Oxygen atoms were placed at hollow sites according to the coverage wanted. The supercells were built in the same way as it was done for the Cu (100) surface. The oxygen atoms were placed at hollow sites and at one Angstrom above the surface in study. The following table shows our result for different coverage.

Table 5-2 Relaxation data for non-reconstructed O/Cu (110)

		$d_0(Å)$	$d_{Cu-O}(Å)$	$\Delta_{12}(\%)$	$\Delta_{23}(\%)$	$\Delta_{34}(\%)$
0.11ML	TW	0.52	2.27	+7.82	-1.1	+3.21
0.5ML	TW	0.53	2.27	+18.86	-4.69	+1.90
0.75ML	TW	0.50	2.21	29.85	-5.44	+1.53
1.0ML	TW	0.082	2.21	+52.80	-5.14	+0.15

5.2.2 Work Function

Our results were compared to the result obtained with the clean surface in the previous chapter. Even though the reconstruction happens before the coverage reaches 1ML, we still considered the coverage starting from 0.25ML to 1ML. The oxygen atoms were placed at the hollow sites of the 2x2 unit cell as described in the previous part. We also used the method used on the average of electrostatic potential. The result of our work can be found in the following table, Table 5.3. The result shows that the work function increases with the oxygen coverage. That can be explained by the fact that as the number of oxygen atoms placed above the surface increases, the negative charges due to the oxygen atoms increase the barrier that make difficult to extract the an electron from the surface.

Table 5-3 Work function change for non-reconstructed O/Cu (110)

Work Function (eV)					
	0ML (clean)	0.25ML	0.5ML	0.75ML	1.0ML
TW		4.29	5.016	5.43	5.79
Work Function Change (eV)					
TW		0.44	0.726	1.14	1.49

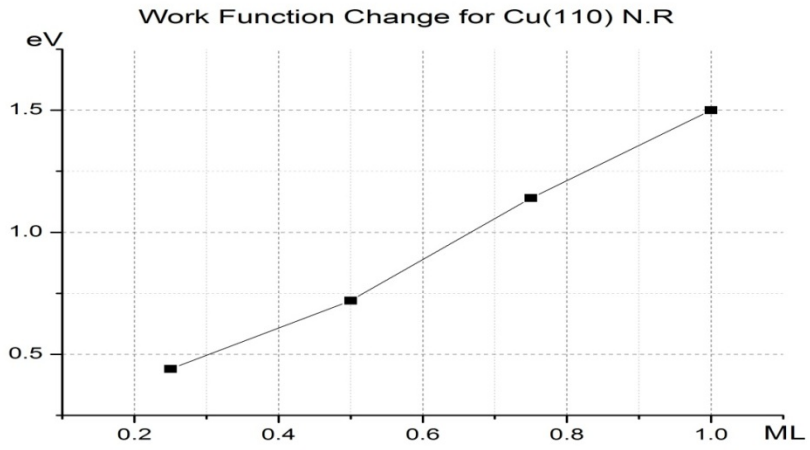

Figure 5-2 Work Function Change for O/ Cu(100)

5.3 Reconstructed O/Cu(110)

5.3.1 introduction

It is accepted and proved today that the oxygen adsorption on the Cu (110) surface may induce a surface reconstruction called “added row reconstruction.” In this reconstruction the (1x1) cell is transformed to (2x1) with oxygen atom placed at bridge sites forming a chain of Cu-O-Cu in the [100] or in [110] direction. Although this kind of reconstruction is accepted many questions remain about the displacement of oxygen and Cu atoms forming the added row relative to their bulk positions. Experimental work including LEED, ICISS, XRD show that the oxygen and the Cu atoms are displaced upwards compared to their positions in the ideal structure.

In this work we focused mainly on the positions that oxygen and copper atoms occupy in the added row structure and the electronic properties of this structure. Because of the geometry of the Cu (110), the Cu-O-chain can be formed in the [100] or in the [110] direction, therefore we have two kinds of added row reconstruction: the [100] added row reconstruction and the [110] added row reconstruction. In the [100] type the oxygen atoms occupy the long-bridge, and in the [110] the short-bridge sites. We were investigated in both structures but we found that the [110] added row is not stable. For low the coverage the binding energy of the [110] change considerably making that structure instable; that was also confirmed by X.Duan [05] in their work. For that reason our work was

focused on the [100] added row structure. The figure (4.6) shows how these two structures are formed from the non-reconstructed (1x1) unit cell. In this part of our work we used the [100] added row to construct the (3x1) and (4x1) super cells in order get 0.33ML and 0.25ML. Figure (5.5) show the top view of the (2X1), (3x1) and the (4x1) super cells we used.

5.3.2 Supercells

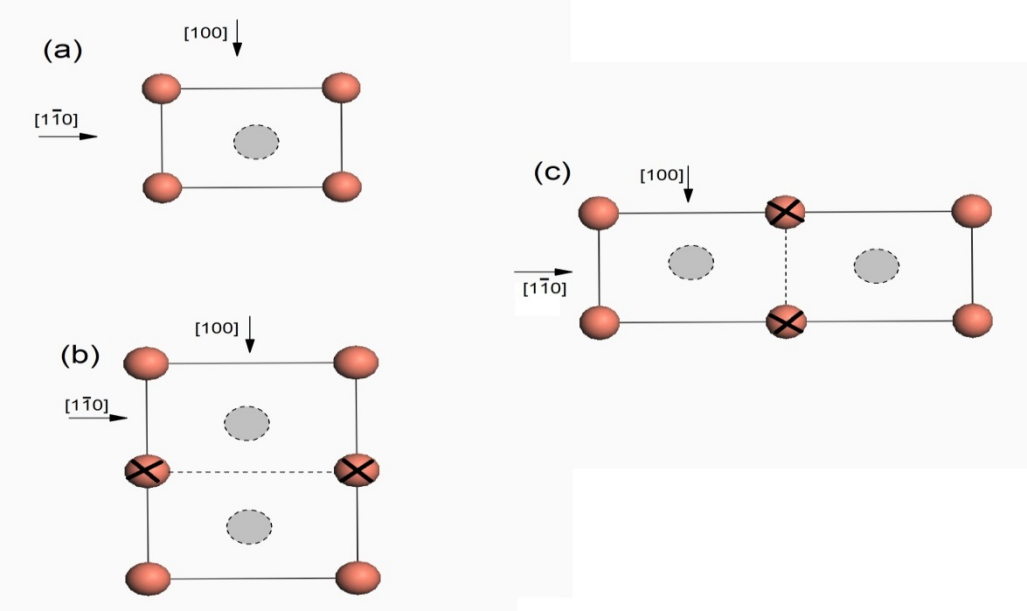

Figure 5-3 Formation of the Added Row Reconstruction

Those figures show how the [100] and [110] super cell are constructed. (a) shows the (1x1) non reconstructed unit cell, (b) corresponds to [100] super cell where the unit cell is doubled in the [100] direction. In (c) the unit cell surface is also doubled but in the [110] direction. The atoms with x sign are deleted to form

one super cell. The X sign on Cu atoms means that those atoms are removed after the reconstruction of the surface.

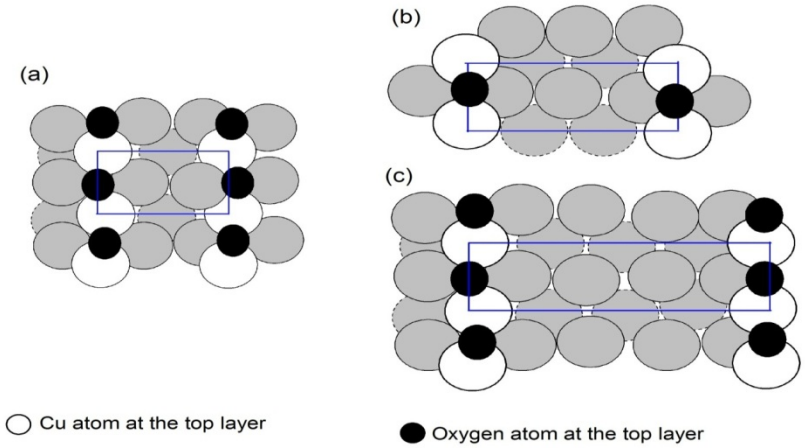

Figure 5-4 Supercells Used for (2x1), (3x1) and (4x1) Added Row Supercells

5.3.3 Relaxation

We used the same method as for clean and O/Cu (100) surface to study the relaxation of the oxygen adsorption on the Cu (110) added row. We used the GGA (p91) as functional, all electrons for core treatment, and DND for basis, and a real space cut-off of 4 Angstroms. The Cu[110] added row structure in which the oxygen atoms occupy the short bridge is not favorable and is much less stable than its counterpart Cu[100] added row. It is characterized by a less binding energy [05]. This can be explained by the fact the repulsion between oxygen atoms is higher because of the short distance separating them. This repulsion leads to O adatoms being displaced significantly outwards. Our attempt to do

calculation with larger cells constructed from the [110] (2x1) added row resulted in unrealistic results. Therefore we concentrated on the [100] added row. The (3x1) and (4x1) cells were obtained from the (2x1) [100] added row by multiplying the short bridge side by three and four as it is shown in the Fig (4.7). These two super cells correspond to 0.3ML and 0.25ML.

The reconstructed surface was built from the relaxed surface by deleting some and expanding the structure in one direction. After the adding the oxygen atoms, the structure was relaxed again to find the stable structure. The following figures show the energy and optimization evolution for the (2x1) added row structure. The convergence was reached after 24 steps.

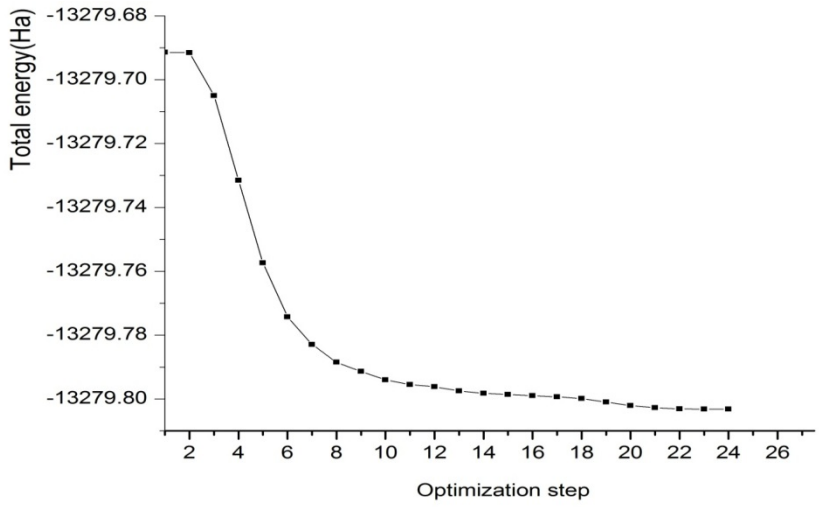

Figure 5-5 Example of geometry optimization

This figure shows how the maximum force on atoms, the maximum displacement of atoms and the maximum energy change during the optimization of the (2x1) added row structure.

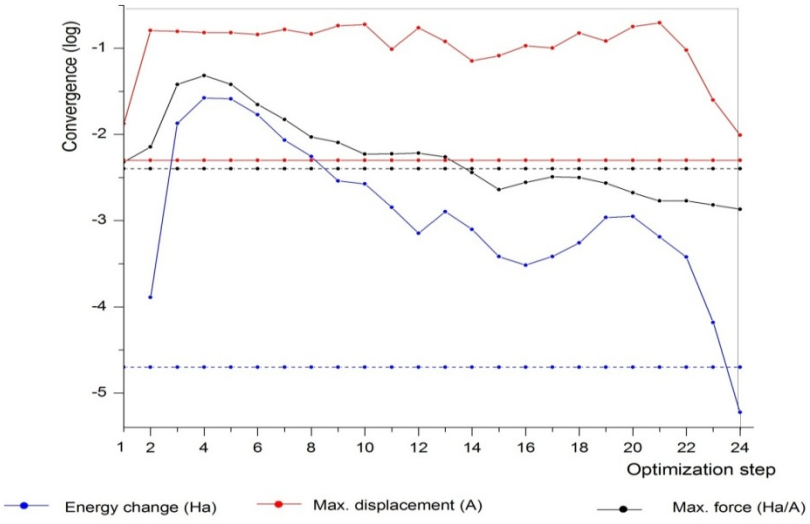

Figure 5-6 Geometry optimization steps

The optimization stopped when at least two of the stopping criteria were satisfied. In this case the maximum energy change and the maximum force (max gradient) criteria were satisfied after 24 optimization steps. The Fig (4.9) shows the total energy evolution for the same structure

In the Table (4.6), we present our results regarding the relaxation of the (2x1), (3x1) and (4x1) supercell. In this table, d_0 is the minimum distance of the oxygen atom above the top layer of Cu atoms, d_{Cu-0} is the average bond length between oxygen atom and the nearest Cu atoms, and the Δ_{ij} is the percent change in the interlayer spacing between the layer I and j. Δ_{ij} is calculated relative to the

relaxed clean surface. That means, $\Delta_{ij} = (d_{ij}' - d_{ij}^{re})/d_{ij}^{re}$ where d_{ij}^{re} are interlayer spacing between layers I and j in the clean bulk, and the d_{ij}' are the average of spacing between layers i and j in the reconstructed structure.

Table 5-4 Relaxation data for added row

		d_0(Å)	d_{Cu-O}(Å)	Δ_{12}(%)	Δ_{23}(%)	Δ_{34}(%)
0.5ML (2x1)	TW	0.1	2.0	+12.2	-2.5	-2.9
	Ref[05]	0.13	1.97	+10.8	-1.5	-3.1
0.3ML (3x1)	TW	0.1	2.1	+13.1	-4.0	-1.0
0.25ML (4x1)	TW	0.1	2.0	+10.0	-4.0	0
	Ref[05]	0.13	1.97	+12.5	-6.4	+0.5

Our calculated values are in good agreement with the reported experimental values [05]. In the (2x1) added row super cell, the oxygen atom is bounded to four Cu atoms, two are surface atoms and the other are under the surface. The d_{Cu-O} is the average bond length of the O atom to the four Cu atom.

5.3.4 Work Function Change

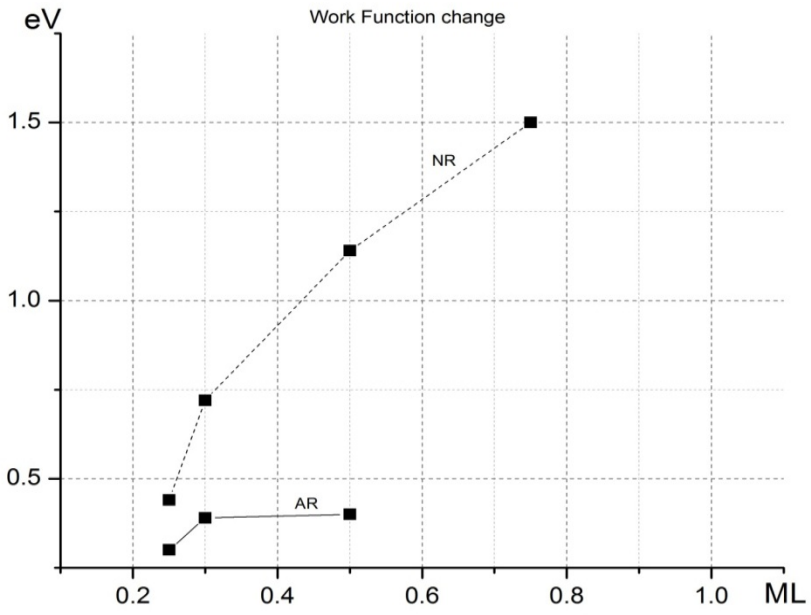

Figure 5-7 Work function change for added row structures

As for the clean surfaces and the O/Cu(100) system we calculated the work function for various oxygen coverage on the Cu(110) surface. The results show the same trend as for O/Cu(100), the work function increases with the coverage.

Table 5-5 Work Function Change for Added Row

Work Function (eV)			
	0.25ML (4x1)	0.33ML (3x1)	0.50ML (4x1)
TW	0.40	0.39	0.31
Ref[05]	0.56		0.33

That is explained by the difference of electronegativity between the Cu atoms and the Oxygen atoms above the top surface. The oxygen atoms are partially and negatively charged due to their bonds with the Cu atom. Therefore this accumulation of negative charge on the above the surface increases the work function.

5.3.5 Mulliken Populations and Charge Transfer

Mulliken populations provide information on how charges are distributed between atoms in the supercell. They give also the total effective number of electrons in each atomic orbital. Here we give our result regarding the (2x1) added row. To understand those data, we need to know how the atoms are arranged in the super layer. That is shown in the figure 5.8. In this figure the #1 and #4 copper atoms are located one on the top layer and the other on bottom layer, and there is charge transfer between each of these two atoms and the O atom that belongs to the same layer. It can be also seen that each oxygen atom on the top and bottom layer has the most negative effective charge compared to the

Cu atoms. The top and bottom Cu atoms have the highest effective positive charge due to their small distance with oxygen atoms.

Mulliken populations:

```
 1 Cu  charge=    0.379
   4 s    0.534
   4 p    0.438
   3 d    9.649
 2 Cu  charge=    0.016
   4 s    0.568
   4 p    0.649
   3 d    9.768
 3 Cu  charge=    0.009
   4 s    0.570
   4 p    0.653
   3 d    9.767
 4 Cu  charge=    0.367
   4 s    0.536
   4 p    0.438
   3 d    9.659
 5 Cu  charge=    0.187
   4 s    0.549
   4 p    0.573
   3 d    9.690
 6 Cu  charge=    0.179
   4 s    0.549
   4 p    0.571
   3 d    9.700
 7 Cu  charge=    0.008
   4 s    0.586
   4 p    0.666
   3 d    9.740
 8 Cu  charge=    0.026
   4 s    0.589
   4 p    0.646
   3 d    9.738
 9 Cu  charge=    0.021
   4 s    0.590
   4 p    0.649
   3 d    9.740
10 Cu  charge=    0.187
   4 s    0.549
   4 p    0.573
   3 d    9.691
11 Cu  charge=    0.179
   4 s    0.549
   4 p    0.571
   3 d    9.700
12 Cu  charge=    0.008
   4 s    0.586
   4 p    0.666
   3 d    9.740
13 O   charge=   -0.791
   2 s    1.848
   2 p    4.900
   3 d    0.043
14 O   charge=   -0.777
   2 s    1.848
   2 p    4.887
   3 d    0.043
```

Mulliken atomic charges:

```
        charge    spin
Cu( 1)  0.379   0.000
Cu( 2)  0.016   0.000
Cu( 3)  0.009   0.000
Cu( 4)  0.367   0.000
Cu( 5)  0.187   0.000
Cu( 6)  0.179   0.000
Cu( 7)  0.008   0.000
Cu( 8)  0.026   0.000
Cu( 9)  0.021   0.000
Cu( 10)  0.187   0.000
Cu( 11)  0.179   0.000
Cu( 12)  0.008   0.000
O ( 13) -0.791   0.000
O ( 14) -0.777   0.000
```

Figure 5-8 Mulliken populations showing charge transfer

Chapter 6

Conclusion

In this work, we studied the change caused by the oxygen coverage on Cu(100) and Cu(110) surface.

Using density functional theory (DFT) within the generalized gradient approximation (GGA) we have studied the stability and associated electronic properties of the oxidized Cu(100) and Cu(110) surfaces. Especially, we have focused on studies of changes in the interlayer spacing, electron work function, and density of states with oxygen coverage.

We have examined the cases of various oxygen coverages of the non-reconstructed, missing row reconstructed Cu(100), and added row reconstructed Cu (110) surfaces. The first-principles calculations in this work have been performed using DMOl3 code. The obtained theoretical results have been compared with available data.

Using the DFT within the GGA approximation, we performed calculations to study the change in the electronic properties of the Cu(100) and Cu(110) surfaces. First we looked at the clean surfaces. In this part, different properties have been examined. Our work confirmed that the copper atomic layers near the surface expand and contract. The Cu(100) layers are characterized by expansion – contraction-expansion, the Cu(110) by expansion – expansion – expansion, the

Cu(111) by expansion – expansion – expansion. This shows that the interlayer spacing depend on the orientation and density of the surface. The work function for the clean surfaces was also calculated and our results are in good agreement with the experimental values and the values reported in some other works. As for the atomic interlayer spacing, the work function depends also on the orientation and concentration of the surface. We found that the Cu(111) surface presents the largest value of the work function followed by the Cu(110) and Cu(111).

The change on electronic properties of the Cu(100) surface due to oxygen adsorption was examined in the second part of this work. Our results were compared to experimental data and they show a good agreement with the experimental and the theoretical values reported by some other authors. Our result show that the change in the interlayer spacing and in the work function depends on the oxygen coverage. The work function increases with the oxygen coverage above the surface. This is due to the increase of an effective negative charge above the surface, and this negative charge transfer is due to charge transfer between oxygen atoms and copper atoms.

In the same chapter we also examined the case of missing row structures. The description of the missing reconstruction and the formation of the super cell were explained. We considered the coverage of 0.5 ML for this structure. The

results on the relaxation and the work function for this structure show also a good agreement with the reported data.

In the last part of this work, we discussed the adsorption of the oxygen on the Cu(110) surface, We considered two structures: the non-reconstructed and the added row structure. For each structure, structure we examined the relaxation and the work function change for different coverage. As for the case of Cu(100) surface we found that the relaxation of the surface depend on the oxygen coverage. Here, also the work function increases with the coverage.

Regarding the added row structure, we found out that the [100] structure is more stable than its counterpart, the [110] structure. We examined the relaxation, the work function and the density of state of the (2x1), (3x1) and (4x1) super cells. Our result also show that our results are in good agreement with experimental and theoretical data.

This study is just a preliminary step of our main work which is the study of the positron annihilation. DMol3 is used only for electron calculation, but we know that what makes the electron different from the positron is just the sign of their charge. Therefore we hope that the understanding of the electronic properties of the surfaces will be useful in our study of positron annihilation on surfaces. At the same time, we will be continuing our effort to master the phenomenon of surface reconstruction since many questions remain unanswered. For example

how deep the adsorbed oxygen atom can go inside the bulk cooper, the reconstruction of the Cu(111) surface due to adsorption of oxygen atom, what cause the Cu(100) surface to reconstruct on Missing Row and the Cu(110) surface on Added Row remain subjects of discussion.

Appendix A

EXAMPLE OF INPUT FILE

```
# Task parameters
Calculate                       optimize
Opt_energy_convergence          2.0000e-005
Opt_gradient_convergence        4.0000e-003 A
Opt_displacement_convergence    5.0000e-003 A
Opt_iterations                  -50
Opt_max_displacement            0.3000 A
Symmetry                        off
Max_memory                      2048

# Cartesian constraints
Opt_fixed
1   XYZ
4   XYZ

# Electronic parameters
Spin_polarization               restricted
Charge                          0
Basis                           dnd
Pseudopotential                 none
Functional                      gga(p91)
Aux_density                     octupole
Integration_grid                medium
Occupation                      thermal 0.10
Cutoff_Global                   4.0000 angstrom
Scf_density_convergence         1.0000e-006
Scf_charge_mixing               0.2000
Scf_iterations                  -50
Scf_diis                        6 pulay

# Kpoint definition file (intervals/offset):
Kpoints                         file     2 4 1 0.0000 0.0000 0.0000
Cu__1_1_0_.kpoints

# Calculated properties

# Print options
Print                           eigval_last_it
```

Figure A-1 Example of input files.

Appendix B

EXAMPLE OF COORDINATES FILE

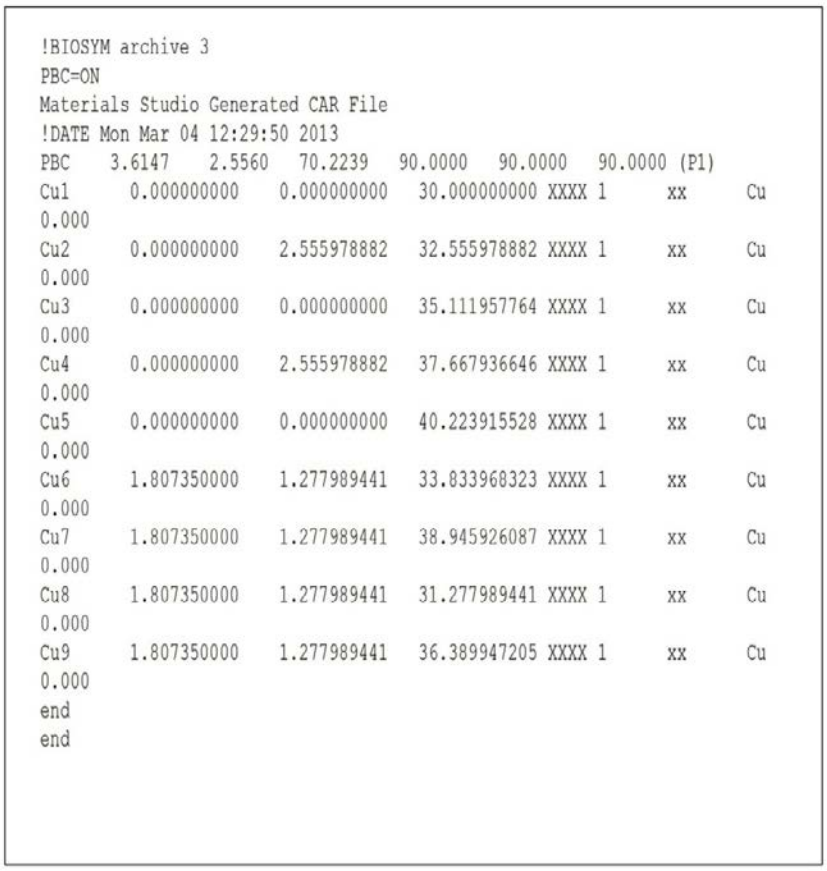

```
!BIOSYM archive 3
PBC=ON
Materials Studio Generated CAR File
!DATE Mon Mar 04 12:29:50 2013
PBC    3.6147    2.5560   70.2239   90.0000   90.0000   90.0000 (P1)
Cu1      0.000000000    0.000000000   30.000000000 XXXX 1      xx      Cu
0.000
Cu2      0.000000000    2.555978882   32.555978882 XXXX 1      xx      Cu
0.000
Cu3      0.000000000    0.000000000   35.111957764 XXXX 1      xx      Cu
0.000
Cu4      0.000000000    2.555978882   37.667936646 XXXX 1      xx      Cu
0.000
Cu5      0.000000000    0.000000000   40.223915528 XXXX 1      xx      Cu
0.000
Cu6      1.807350000    1.277989441   33.833968323 XXXX 1      xx      Cu
0.000
Cu7      1.807350000    1.277989441   38.945926087 XXXX 1      xx      Cu
0.000
Cu8      1.807350000    1.277989441   31.277989441 XXXX 1      xx      Cu
0.000
Cu9      1.807350000    1.277989441   36.389947205 XXXX 1      xx      Cu
0.000
end
end
```

Figure B-1 Example of input file

References

[01] Michael P. Murder, Condensed Matter Physics”

[02]C. Kittel, Introduction of Solid State Physics Wiley, New York, (1996).

[03] Monkhorst, H. J.; Pack, J. D. "Special points for Brillouin-zone integrations", Phys. Rev. B, 13, 5188-5192 (1976).

[04] Willie Burton, “Theoretical Study of Electronic Properties of the Cu(001) Surface under Conditions of High Coverage Oxidation”

[05] X. Duan , O. Warschkow, A. Soon, B. Delley, and C. Stampfl “Density functional study of oxygen on Cu(100) and Cu(110) surfaces”

[09]X. M. Tao, M. Q. Tan, X. X. Zhao, W. B. Chen, X. Chen, and X. F. Shang, Surf. Sci. 600, 3419 2006.

[10]R. Mayer, C. S. Zhang, K. G. Lynn, W. E. Frieze, F. Jona, and P. M. Marcus, Phys. Rev. B 35, 3102 1987.

[11] J. Wan, Y. L. Fan, D. W. Gong, S. G. Chen, and X. Q. Fan, Modell. Simul. Mater. Sci. Eng. 7, 189 1999.

[12]H. L. Davis and J. R. Noonan, Surf. Sci. 126, 245 1983.

[13] J. L. F. Da Silva, K. Schroeder, and S. Blügel, Phys. Rev. B 69**,** 245411 2004.

[14] Aloysius Soon,1,* Mira Todorova,1 Bernard Delley,2 and Catherine Stampfl1 PHYSICAL REVIEW B 73, 165424 (2006)

[15] S. A. Lindgren, L. Walldén, J. Rundgren, and P. Westrin, Phys. Rev. B 29, 576 (1984).

[16] S. P. Tear, K. Röll, and M. Prutton, J. Phys. C 14, 3297 (1981).

[17]P. O. Gartland, S. Berge, and B. J. Slagsvold, Phys. Rev. Lett. 28, 738 1972.

[18]P. O. Gartland, S. Berge, and B. J. Slagsvold, Phys. Rev. Lett. 28, 738 1972.

[19]H. L. Skriver and N. M. Rosengaard, Phys. Rev. B 46, 7157

[20] K. W. Jacobsen and J. K. Norskov. Theory of the oxygen-induced restructuring of cu(110) and cu(100) surfaces. Phys. Rev. Lett., 65(14):1788-1791, Oct 1990.

[21] E. A. Colbourn and J. E. Inglesfield. Effective charges and the surface stability of o on cu(001). Phys. Rev. Lett., 66(15):2006-2009, Apr 1991.

[22] Sergey Stolbov and Talat S. Rahman. Relationship between electronic and geometric structures of the o/cu(001) system. The Journal of Chemical Physics, 117(18):8523-8530, 2002.

[23] J. L. F. Da Silva, C. Stampfl, and M. Scheffler. Converged properties of clean metal surfaces by all-electron first-principles calculations. Surface Science, 600(3):703 - 715, 2006.

[24] K. P. Rodach, T. Bohnen and K. M. Ho. First principles calculations of lattice relaxation at low index surfaces of cu. Surface Science, 286(1-2):66-72, 1993. Gary G. Tibbetts, James M. Burkstrand, and J. Charles Tracy. Electronic prop-erties of adsorbed layers of nitrogen, oxygen, and sulfur on copper (100). Phys.Rev. B, 15(8):3652-3660, Apr 1977.

[25] P. O. Gartland, S. Berge, and B. J. Slagsvold. Photoelectric work function of a copper single crystal for the (100), (110), (111), and (112) faces. Phys. Rev.Lett., 28(12):738{739, Mar 1972.

[26] J. G. Gay, J. R. Smith, and F. J. Arlinghaus. Large surface-state/surface-resonance density on copper (100). Phys. Rev. *Lett.*, 42(5):332{335, Jan 1979.

[27] T. Lederer, D. Arvanitis, G. Comelli, L. TrÄoger, and K. Baberschke. Adsorption of oxygen on cu(100). i. local structure and dynamics for two atomic chemisorption states. Phys. Rev. B, 48(20):15390-15404, Nov 1993.

[28] T. Kangas, K. Laasonen, Puisto A., H. Pitknen, and Alatalo M. On-surface and sub-surface oxygen on ideal and reconstructed cu(100). Surface Science, 584(1):62 { 69, 2005. Selected papers of the Fifth Nordic Conference on Surface Science (NCSS-5).

[29] M. Kittel, M. Polcik, R. Terborg, J. T. Hoeft, P. Baumgrtel, A. M. Bradshaw, R. L. Toomes, J. H. Kang, D. P. Woodru®, M. Pascal, C. L. A. Lamont, and E. Rotenberg. The structure of oxygen on cu(100) at low and high coverages. Surface Science, 470(3):311 { 324, 2001.

[30] U. DÄobler, K. Baberschke, J. StÄohr, and D. A. Outka. Structure of c(2x2) oxygen on cu(100): A surface extended x-ray absorption ne-structure study. Phys. Rev. *B*, 31(4):2532-2534, Feb 1985.

[31] K. W. Jacobsen and J. K. Norskov. Theory of the oxygen-induced restructuringof cu(110) and cu(100) surfaces. Phys. Rev. Lett., 65(14):1788{1791, Oct 1990.

[32] J. G. Tobin, L. E. Klebanof, D. H. Rosenblatt, R. F. Davis, E. Umbach, A. G. Baca, D. A. Shirley, Y. Huang, W. M. Kang, and S. Y. Tong. Normal photoelectron diffraction of o/cu(001): A surface-structural determination. Phys. Rev. B, 26(12):7076-7078, Dec 1982

Biographical Information

Antoine Olenga was born in Democratic Republic of Congo where he received his bachelor's degree in physics before he moved to United States in 2002. He has been a graduate student in Department of Physics of UTA since Fall 2010. Before he came to UTA he worked as researcher at The Center for Nuclear Studies of Kinshasa/Congo (CRNK) and an International Atomic Energy Agency (IAEA) fellow at the University of Texas at Austin. Now he is working towards his PHD degree in physics at UTA. His area of interest is Theoretical Condensed Matter Physics.